MASTER THESIS

Rain erosion performance of the material to be used as the leading edge protection of the wind turbine blades

Udaya Aditya Ghantasala (s2086751)

Faculty of Engineering Technology

Mechanical Engineering

Department of Production Technology

Prof. Dr. Ir. R. Akkerman

Examination committee:

Dr. Ir. T.C. Bor (chairman)

Dr. I. Baran (supervisor)

Ir. T.H. Hoksbergen (supervisor)

Dr. Ir. T.H.J. Vaneker (external member)

Document number

MS3/PT-0061

Enschede

19/03/2021

UNIVERSITY OF TWENTE.

Acknowledgements

It gives me immense pleasure to sincerely acknowledge the people who helped me in different ways to complete my thesis at University of Twente. Firstly, I thank dr. I. Baran for accepting my request to perform thesis in the Department of Production Technology. It is a matter of pride, pleasure, and prestige that I could work for a group which is very passionate about manufacturing process and the performance of lightweight materials in structural applications.

I would like to express my deepest gratitude to my supervisor, ir. T.H. Hoksbergen, for taking his valuable time out and giving me insightful suggestions and recommendations. On-spot guidance and the company given by him during the experimentation, and all the casual talks have made me feel comfortable during this research.

I further thank ing. N.G.J. Helthuis for helping me in working with the VK9710 Keyence confocal microscope in the microscopy lab at the University of Twente. Also, I am pleased to gratify the resources and access provided by University of Twente that helped in performing the thesis effectively.

I would like to express my gratitude to my parents, G.V. Chakradhara Rao and K.P. Vardhani for the support especially during the past few years. Finally, I would like to thank my friends at the University of Twente and from India for making life during my masters more cheerful.

Udaya Aditya Ghantasala

Abstract

In recent years the size of wind turbine blades is growing rapidly which increases their tip speeds over 110 m/s. When these blades are being operated, they are exposed to continuous impacts with rain droplets, hails and insects. This leads to the erosion of the blade causing significant loss in aerodynamic efficiency of the wind turbine blade resulting in considerable reduction of annual energy production. Timely and expensive, maintenance and repair works are required to control the progression of damage. One of the possible solutions for this problem is to develop an integrated leading-edge protection (InLEP) for the leading edge of the wind turbine blades to protect the blade from erosion.

This research project studies the rain erosion performance of the materials used for the leading edge of the wind turbine blades. A pulsating jet erosion test (PJET) setup available at the University of Twente was used to conduct the erosion tests on Acrylonitrile Butadiene Styrene (ABS) thermoplastic material. The most important parameters of the PJET setup such as nozzle diameter, impact velocity, impact frequency and angle of impact were kept constant throughout the research. A pump pressure of 160 bars with an output nozzle diameter of 1.0 mm was used to achieve a water stream with a velocity of 175 m/s which was then cut into jet slugs by using a rotating disc which rotates at a speed of 600 rpm. These jet slugs further travel to hit the specimen at an impact angle of 90^0 with the vertical at a frequency of 200 Hz.

To identify the occurrence and development of the erosion in the ABS material due to the rain droplet impacts, a set of experiments ranging from 200.000 to 1.200.000 impacts were conducted and the height maps of the eroded specimens were obtained by using a Keyence VK9710 laser scanning confocal microscope. A methodology for analysis of these eroded samples was created using volume loss algorithm and skewness (Ssk) surface roughness parameter. It was identified that the end of the incubation of ABS material was just after the 600.000 impacts with a short acceleration phase until 800.000 impacts. To analyse the effect of water layer on the sample on the rain erosion, a similar set of experiments was conducted with a water layer removal system installed to the PJET setup, which blows compressed air at 2 bar pressure through a flat air nozzle. The effect of the water layer was evident as the end of incubation phase was observed before 400.000 impacts and a huge crater was found on the surface of the specimen at 600.000 impacts which suggests the end of acceleration phase. The volume loss at 1.200.000 impacts in the case of tests with air blower is 4.6 times higher than that of the volume loss at 1.200.000 impacts in the case of without water layer removal system.

To study the influence of additional strains in the material on its rain erosion performance, the fixture clamp was modified in order to induce a tensile loading on the specimen. When a 3% strain was induced on the sample, after 170.000 impacts the volume loss on the surface of the material and the

intensity of pits in this case was higher than that of compared to the 200.000 impacts test performed without a water layer removal system.

From this research it was concluded that the material possesses a very short acceleration phase which leads it to enter the maximum erosion state in short duration after the end of its incubation phase. The end of incubation phase of the ABS material was identified after 600.000 impacts when there is a water layer on the sample and at 400.000 impacts when a water layer removal system was employed. The rain erosion performance of the ABS material was influenced when either of additional strains were induced on the sample or a water layer removal system was employed to the PJET setup.

Contents

Nomenclature

RES	Renewable Energy Sources
LCOE	Levelized Cost of Energy
HAWT	Horizontal Axis Wind Turbine
InLEP	Integrated Leading Edge Protection
LEP	Leading Edge Protection
PJET	Pulsating Jet Erosion Test
RET	Rain Erosion Test
Sv	Maximum pit depth of an area
Rv	Maximum pit depth of a line
Sp	Maximum peak height of an area
Rp	Maximum peak height of a line
Sz	Maximum height of an area
Rz	Maximum height of a line
Ssk	Skewness of an area
Rsk	Skewness of a line
Sku	Kurtosis of an area
Rku	Kurtosis of a line
Sq	Root mean square height of an area
Rq	Root mean square height of a line
Sa	Arithmetic mean height of an area
Ra	Arithmetic mean height of a line

List of Figures

List of Tables

1 Introduction

The desire of mankind to meet the continuously growing demands forced us to look out for different sources of energy. The various energy sources are majorly divided into three categories,

1. Fossil fuels
2. Renewable energy sources
3. Nuclear resources

The demand for renewable energy sources (RES) is growing rapidly amid the concerns of global warming and greenhouse gas emissions caused by the fossil fuels. In recent years among the EU-28 countries there is a significant raise in the electricity generation utilizing the RES such as wind and solar. Between the years 1997 and 2019 the contribution of electricity production from the developing RES technologies has grew from less than 1% to about 42% with wind energy contributing over 31%, see Figure 1 [1].

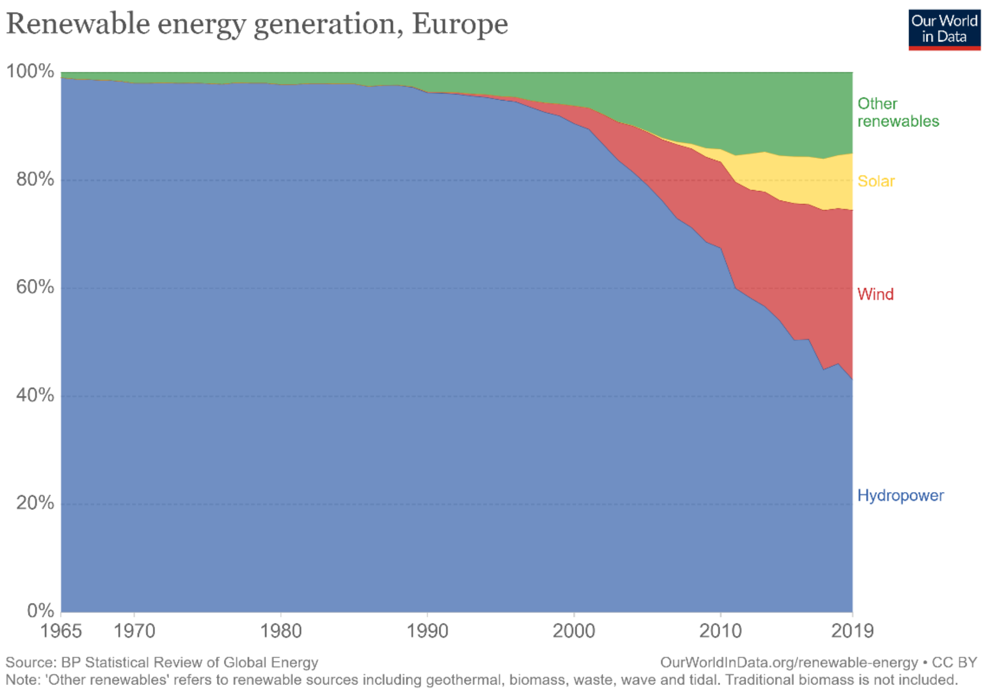

Figure 1 Development of electricity from RES in Europe between 1965 and 2019 [1]

From 2016 to 2018 the wind energy sector has seen rapid growth of 25.2% in its annual electricity production [2]. In addition, the EU has further set an ambitious target of a share of 27% energy from renewable energy sources by 2030, which clearly indicates that the electricity production in the wind sector especially offshore has a crucial role to play in order to achieve this goal as the size of size wind turbines is growing rapidly.

Including the conventional energy sources such as coal and gas, wind energy is the cheapest available source of electricity generation in majority of places in the world. In the first half of 2018, the levelized cost of energy (LCoE) of onshore wind in Europe ranges from €50 to €65/MWh. Onshore wind is the cheapest energy source in Europe and the world when the pollution costs and subsidies were taken into account which were not included in the LCoE estimations. Offshore wind energy is costlier than the onshore wind. Cost reduction techniques depending on the pipeline projects are being studied in the field of offshore wind in order to reach a goal of €60/MWh by 2025 [3].

1.1 Introduction to the Wind turbines

A mechanical device is required to convert energy from one form to the other. In this particular case the kinetic energy of wind is to be transformed into the mechanical power which later is converted into electric power by using a generator. The device which is used for the transformation is called as a wind turbine. Wind turbines can be used to generate large amounts of energy both offshore and onshore. The most common design of the wind turbine and the type which is focused in this report is a horizontal axis wind turbine (HAWT) where the axis of rotation is parallel to the ground. The subsystems of a wind turbine can be seen in the Figure 2Subsystems of a wind turbine [4]. This report focusses on the wind turbine blades and more specifically the leading edge.

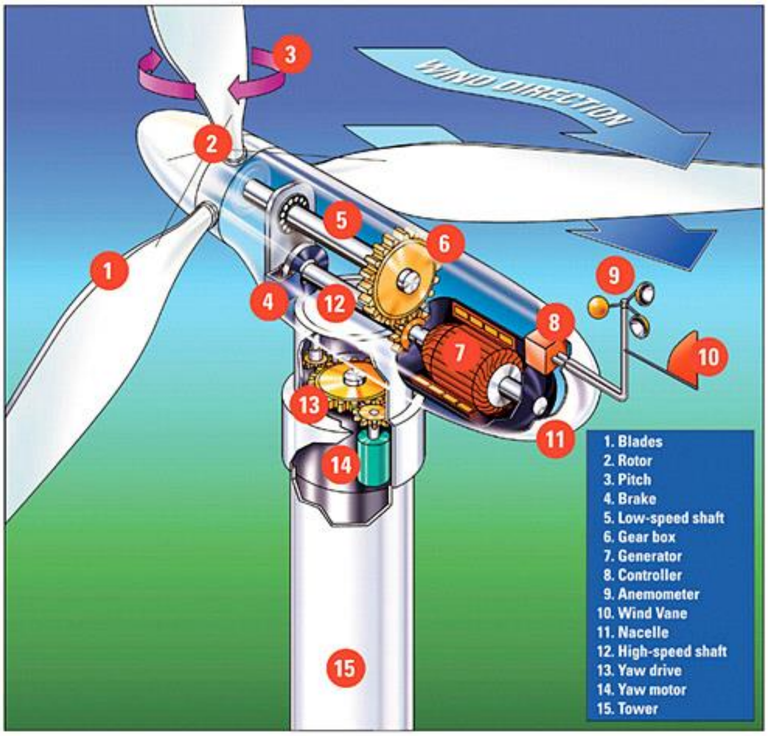

Figure 2 Subsystems of a wind turbine [4]

Wind turbines are considered a mature technology and are provided commercially in a wide range of capacities from 400 W to 12 MW [5]. The theoretical maximum aerodynamic conversion efficiency of wind turbines from wind to mechanical power is 59%. However, in reality the peak efficiency is about 45%. The average annual efficiency of most turbines is about half this number because of the need to shut down the wind turbine in low or high winds and to limit the power once the rated level is reached. It may also be caused by generator loss and the fact that the machine does not always operate in its optimum working point [6].

The bigger the turbine blade, the higher the capacity of the wind turbine. The world's largest wind turbine is "Haliade-X" manufactured by GE Renewable energy whose rotor diameter is about 220 meters with a capacity of 12MW [7]. The wind turbine looks simple, but there are many under lying design concerns, technical issues and real-time working concerns which went unanswered. Researchers have been trying to solve some of the problems over the years to make them more sustainable. Lightning strike, flapping of the blades, mechanical breakdown, icing and leading-edge erosion are some of the common problems faced by the wind industry.

1.2 Assignment Description

A wind turbine is designed to serve a life span of 20-25 years. During their operational time the components of wind turbines (especially the rotor blades) are exposed to unforeseen extreme environmental conditions such as heavy rainfall and hailstorms. These raindrops and hailstones deteriorate the leading edge of the blade drastically resulting in the removal of material from the surface of the blade which creates a rough profile impacting the structural integrity of the blade. Eroded leading edge of a wind turbine blade can be seen in Figure 3.

Figure 3 Eroded leading edge of a wind turbine blade [8]

As the tip speeds are increasing constantly and the offshore wind industry has been moving to new markets with monsoonal climates, the leading-edge erosion problem has its own impact on the electricity production. It has progressed from a single wind turbine issue to a problem which affects the entire wind farm. The performance of a wind turbine is largely dependent on the aerodynamic properties of its blades. Leading edge erosion results in reduced aerodynamic efficiency which diminishes the output electricity production and reduces the availability of the turbine. It also increases the drag on the blade, a mild erosion can create an additional 6% of drag and it can be increased to a 500% in the case of a severely eroded blade [9]. The eroded wind turbine blade requires expensive repairs which increases the cost of maintenance and gradually decreases the lifetime of the blade. In Figure 4 a picture of wind tech applying coatings to the leading edge of the wind turbine blade can be seen.

Figure 4 Turbine blade undergoing Maintenance [10]

To develop an Integrated Leading-Edge Protection system (InLEP (Drachmann and LM Wind Power Patent Holding A/S, 2017)), University of Twente has collaborated with LM Wind Power who are one of the leading manufacturers of wind turbine blades. The main goal of this project is to develop an enhanced and long-lasting hybrid LEP concept, integrated in the blade structure. Usually, the blades are made up of thermoset materials, in this project it is intended to use thermoplastic materials for the leading edge of the blade to protect it from erosion as the properties of thermoplastics are suitable to withstand for higher range of impacts. The integration of the LEP layer in the blade structure should result in better aerodynamic and rain erosion performance for offshore wind turbines, reducing the Levelized Cost of Energy (LCoE) of wind energy by 6%.

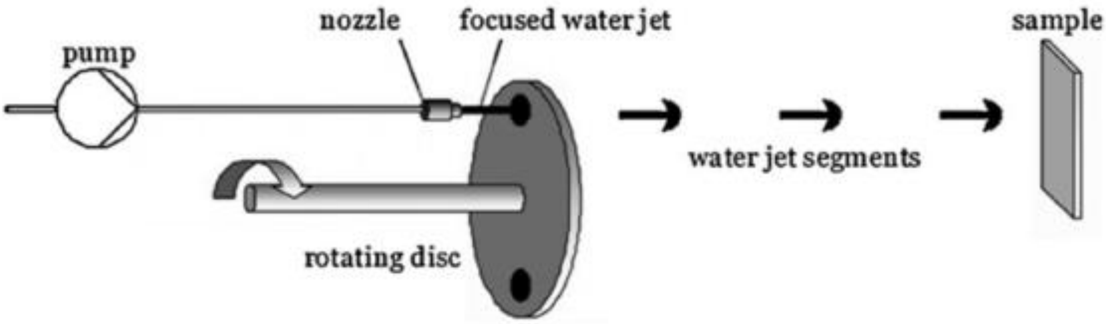

Figure 5 Principle of PJET setup [11]

It requires vigorous study to validate a thermoplastic material for using it in massive structures like a wind turbine. To figure out the best suited thermoplastic material for the InLEP project, a variety of circumstances need to be assessed. A Pulsating Jet Erosion Test (PJET) setup has been developed by the Production Technology group at University of Twente which will be used to identify the behaviour of thermoplastic materials when subjected to impingement of rain droplets [12]. The working principle of PJET setup can be seen in Figure 5. Research needs to be conducted in order to analyse the damage occurrence and its propagation in the materials over the course of time.

1.3 Outline of subsequent chapters

Chapter 2 elaborates the research state of the art, important parameters and new trends in protecting the blades from leading edge erosion whereas chapter 3 covers the experimental methodology used to answer the research questions of this project. Chapter 4 addresses the methodology used to perform the analysis of the results obtained from the rain erosion experiments. Chapter 5 presents the various approaches followed to reduce the elapsed time for experimental work. In chapter 6, the result analysis of the rain erosion tests of the material used for the leading-edge protection of the wind turbines was covered. Chapter 7 details the effect of additional strain on the rain erosion performance of a material. In chapter 8, the conclusions extracted from this research were briefly described and chapter 9 highlights the scope for future work.

2 Literature Review

This chapter describes the current state-of-the-art with respect to the leading-edge erosion of wind turbine blades. The first part of this chapter contains an overview of the leading-edge erosion of a wind turbine blade. The second part contains a brief discussion regarding the physics behind the droplet impact, then followed by the contemporary solutions in the field. The fourth part discusses about different RET setups used for research purposes. The last part consists of an overview of the most important parameters that influence the rain erosion on the leading edge of a wind turbine blade.

2.1 Leading Edge Erosion

Sometimes the erosion damage can be seen in different parts of a wind turbine blade, but it is very substantial in the leading edge of blade. The leading-edge erosion is directly dependant on the rotational speed of the wind turbine. The erosion is drastic at the tip of the blades compared to that of at the root of the blade because the rotational speed of the turbine blade linearly decreases from tip to the root. This phenomenon can be observed in Figure 6. In the preliminary stages of the erosion only minor pitting on the coating can be observed, while in the next stage the underlying epoxy is visible. In the later stages of the erosion, the top coating is completely removed and later on the damage is severe with the formation of craters which are over 15 mm deep [13].

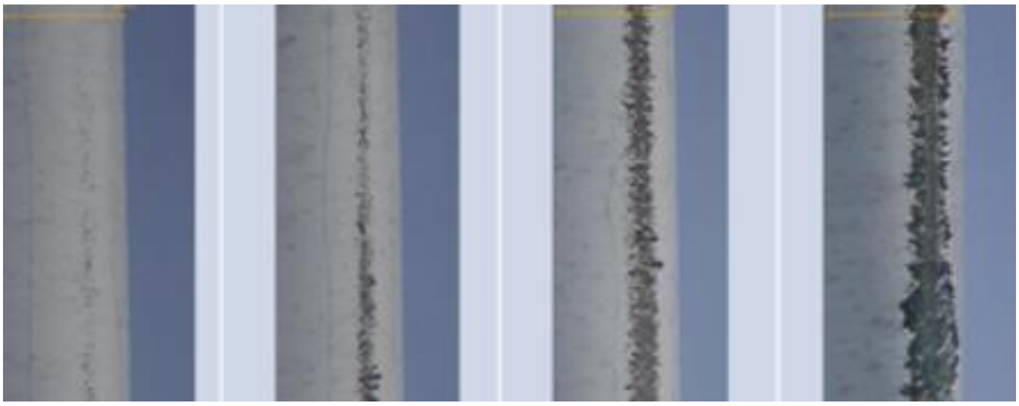

Figure 6 Level of erosion damage experienced at different radii [13]

Due to the leading-edge erosion the aerodynamic efficiency of the turbine blades is considerably reduced which results in significant reduction in annual energy production. Studies show that a highly eroded wind turbine blade can be subjected to an increase of drag by 500% and decrease of lift by 53% which can result in a 20% reduction in the rated power of the turbine [13].

2.1.1 Time dependency and stages of erosion

Experimentations over the past years have revealed that the water droplet erosion is a time dependent phenomenon which exhibits different erosion rates at different time intervals, resulting in a nonlinear progression of damage which can be classified into five stages [13]. Figure 7 shows the erosion level of Ti-6Al-4V alloy to represent the various stages of erosion. The first stage is called as the incubation period in which surface roughness of the material increases due to the repetitive impact of the water droplets with a very negligible material loss. Later on, at the end of incubation with the emergence of micro pits, a measurable material loss can be identified. During the further impacts, the material loss keeps on increasing which is called as the acceleration stage. In this stage the intensity of pits increases which leads them to combine with one another and grow into a crater. By the end of the acceleration stage the rate of erosion increases to its maximum and remain constant over a long duration. This stage is known as the steady-state maximum erosion rate. When the crater formed due to erosion reaches certain depth, the rate of erosion starts decreasing. This particular stage is called as deceleration stage where the rate of erosion is usually 25% to 50% of that of the maximum erosion rate. Irregularities and high roughness of the erosion crater is one of the main reasons for the deceleration of the rate of erosion. This stage continues until it becomes constant in terminal stage. Post deceleration stage, the rate of erosion rapidly increases in some of the brittle materials which leads to catastrophic stage.

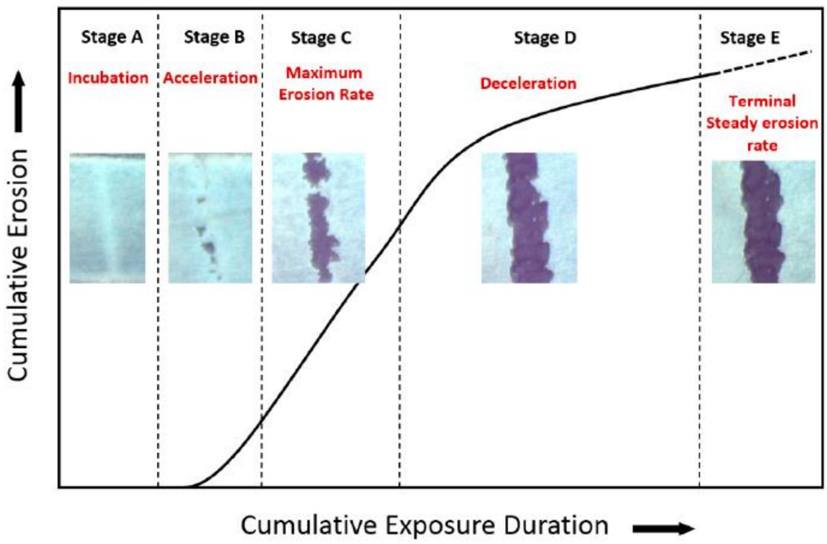

Figure 7 Typical stages in water droplet erosion damage curves with an example of Ti64 tested at 300 m/s impact velocity with droplets of 460 µm size [13].

In a practical point of view, the end of incubation and acceleration stages are the most important phases of the erosion damage as at this stage the components are easily serviceable and necessary precaution can be employed to prevent further damage.

2.2 Physics of Droplet Impact Erosion

Droplet erosion is one of the different forms of material wear which is caused due to the impact of liquid droplets at a high speed which is also called liquid impingement erosion. In very aggressive conditions even highly wear resistant materials will suffer damage. The phenomenon of degradation of materials due to the impingement of water droplets at high velocities is well-known in different environments such as aircraft components, steam turbines and wind turbine blades.

As seen in Figure 8 when the impact of a water droplet is normal to the surface of the material, a compressional shock wave is generated and it propagates through the material. The increase in the contact area between the droplet and the material results in the generation of shear waves which propagate away from the location of impact through the material. These intensive stress waves produce damage at the point of impact. The propagation of these waves is very much dependant on the acoustic impedance of the material which alters from one material to the other based on its stiffness and hardness. A material with high impedance is not recommended as a protection system, as it absorbs more amount of wave energy leading to cracks and other forms of erosion damage, whereas a material with low impedance transmits more amount of wave energy through its thickness [14]. The materials with high impedance also have higher strength. The material to be used as a protection system should have a balance between the strength and elastic properties.

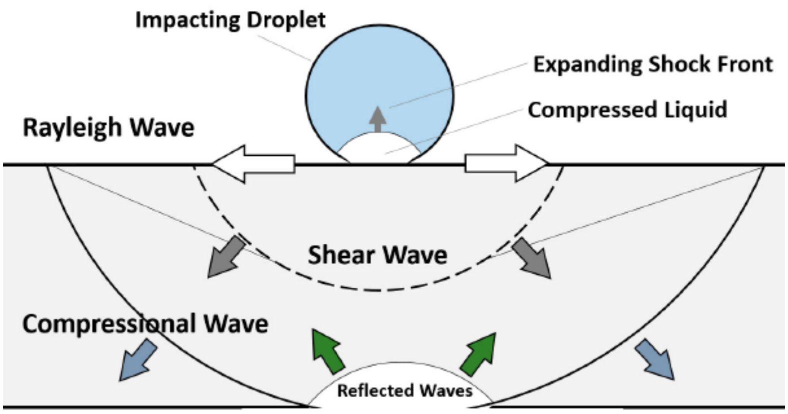

Figure 8 Schematic representation of shock wave behaviour during the liquid droplet-solid surface interaction [13]

The erosion caused by the impact of the rain droplet can be divided into two phases. The first phase commences when the droplet directly hits the surface of the material and this leads to cracks and deformation in the material. The other phase is when the high velocity lateral water jets start effecting the irregularities on the surface. When the droplet hits the solid surface, within the droplet a compressed liquid wave front travels in the upward direction. The droplet collapses and lateral jets with a speed up to 40 times the speed of the impact, when the liquid wave front spreads past the contact periphery between the droplet and surface. The amount of lateral jetting is directly dependant on the surface hardness and it spreads radially outwards from the location of impact. A hard material will reflect large portion of the initial impact energy back into the droplet which results in high lateral jetting, whereas a soft material deforms by absorbing the energy from the impacts which reduces the energy reflected into the droplet resulting in reduced lateral jetting [14].

Elasticity and viscoelasticity of the material determines the short term and long-term recovery of the materials respectively. The damage mechanisms on a smooth surface are confined to stress wave propagation and direct deformation. However, when the surface the material becomes rough, it is highly affected by the lateral jetting process [14]. For polymeric materials, the erosion initiation and progression can be explained as a resultant of one or more of the following mechanisms [13]:

- Direct deformation at high-speed impacts.
- Stress wave propagation.
- Surface fatigue due to the continuous droplet impacts.
- Erosion can be caused due to lateral jetting on a rough surface with initial pits due to former impacts.
- During heavy rain, the frequency of droplet impacts is as high as it does not allow the material to recover completely from the previous droplet impact.

2.3 Contemporary Solutions

In the current scenario to a certain extent the leading-edge erosion of wind turbine blades is dealt by coatings. The coatings are meant for protection of composite material from environmental factors such as UV radiation, insects, moisture and foreign body impacts like rain drops and hails. The small additional costs with leading edge protection are estimated to be worthwhile throughout the life of a wind turbine [15].

In general coatings are used to aid surface protection for structures built with organic and/or inorganic chemicals. Resin, solvents, pigments and additives are the major constituents of the liquid coating materials which are allowed to cure. There are two methods of surface coating applications. A brief description on the coating applications has been provided in this subchapter.

2.3.1 In-mould coating

As the name suggests in the In-mould coating technique the coatings are applied to the leading edge while the blades are still in the mould, during the moulding process. In this technique the material used for the coating should be similar to that of the matrix material of the blade to bind well with the blade. In general epoxy or polyester is used as matrix material [12]. The main advantage of this technique is that it is easily integrated in the blade and reduces the cost of applying coatings after moulding.

2.3.2 Post-mould coating and tapes

These types of coatings are applied to the blade after the moulding process by painting or spraying whereas the tapes are attached using adhesives. The coating application is flexible with different materials to choose from like polyurethane whereas the procedure is designed based on the final material properties such as thickness, surface roughness, etc. Post mould coatings or tapes are preferred for leading edge repairs, during which the manufacturers use putty or primer layers between the blade and the coating. Longevity of these coatings are highly dependent on environmental conditions [12].

2.3.3 Reduction of tip speed

Another approach to control the rain erosion is by reducing the speed of the blade tip during heavy precipitation which is one of the major reasons for the erosion. The tip speed of the blades can be adjusted by using a precipitation sensor which measures the intensity of the rain, so that the blades are not prone to severe damage. By following this method, the loss of income which is calculated based on the Total Energy Production, Energy Cost, Number of Repairs, Costs of Repairs and Costs of Inspections can be reduced from 15.4% to 4.5% [12]. It is very challenging to predict the accurate amount of precipitation. Therefore, this method can be used together with a coating material to increase the lifetime of the wind turbine blade. However, the wind turbine could generate more energy at higher blade tip speeds.

2.4 Rain erosion test methods

Severe erosive conditions are artificially generated during the rain erosion tests to produce rapid erosion damage. Due to the lack of correlations between the testing environment and actual work conditions, quantitative prediction of the erosion has not yet been to a precise level. Therefore, by utilizing these erosion tests a qualitative assessment of erosion behaviour is the best possible study to understand the erosion behaviour. Whirling arm and jet erosion test are the two main rain erosion test methods. In this subchapter a brief overview of RET setups has been provided.

2.4.1 Whirling arm setup

In recent years the whirling arm test setup has been used for testing of wind turbine blade coatings and it is also a recommended practice by DNV-GL-RP-0171 for testing of rotor blade erosion protection systems [16]. The principle of whirling arm to test the rain erosion behaviour was developed by the Radiation Laboratory at MIT in 1946. In this method the test specimens are mounted on a horizontal arm which rotates in artificial rainfall. The results of this method are closely matched to the results of actual flight tests. Figure 9 shows whirling arm setup at the University of Limerick.

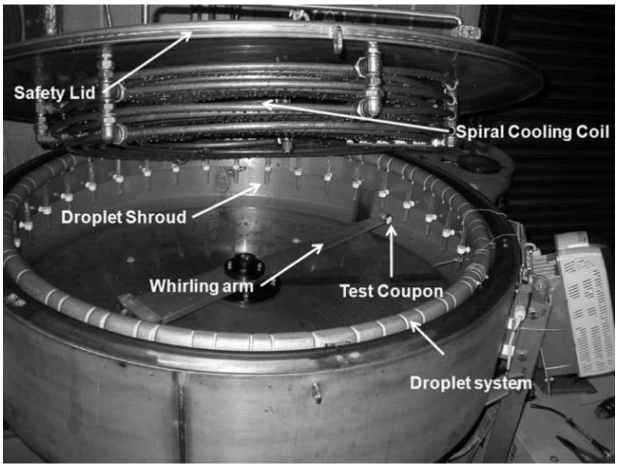

Figure 9 Main Components of a whirling arm setup [17]

The whirling arm test setups are used in the aviation industry where the raindrop impact is in horizontal direction on the airplane wings and helicopter blades. The rotation of wind turbine is vertical which causes more complex raindrop impacts. When the blade is at its highest position the impact of the rain drop is along the leading edge in direction to the rotor. This makes the whirling arm test facilities not a suitable option to replicate the actual movement of the blades under rainfall [18]. These whirling arm tests can be used to compare erosion resistance of different materials, but the failure mechanism differs from the real time wind turbine blades as the impact physics differs from one another.

2.4.2 Jet based setup

Out of all the available jet-based RET setups, the results obtained by Pulsating Jet Erosion Test (PJET) are promising and more reproducible as the size of the droplet, impact frequency and impact area are easily controllable while working with the PJET when compared with other jet-based setups [18].

The PJET setup is based on high-velocity jet slugs which impact the test specimen in a controlled manner. In contradiction to the whirling arm setup, the specimen is stationary and the water jet moves in the PJET setup. A rotating disk with slots creates jet slugs when the water jet passes through the slots. A high-pressure pump and nozzle are used to achieve the required jet velocity and the size of rain drop. Figure 10 shows the working principle of PJET setup.

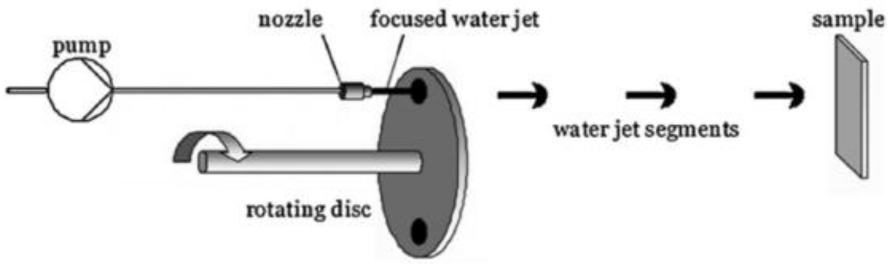

Figure 10 Working Principle of PJET- setup [17]

The velocity of the water jets can be altered by varying the water pressure of the pump whereas the size of the droplets can be varied by varying the diameter of the nozzle. The hose length between the pump and the nozzle should be long enough in order to compensate the pressure variations in the pump [17]. A pump pressure of 100 bar and 150 bar results in a water jet velocity of 140 m/s and 167 m/s respectively [15].

2.4.3 Comparison of RET setups

Results of the both RET methods in a previous research using a clad (AA1230) aircraft grade aluminium alloy (AA2024-T3) sample are correlated and it can be inferred that the PJET setup can provide valuable data on the relative resistance of different samples. For this specific research, approximately a 1000 PJET impacts can be correlated with 15 minutes of whirling arm testing. The material loss of the samples has been observed after 30 minutes of testing with whirling arm, which is equivalent to 2000 impacts at a droplet speed of 177 m/s with the PJET setup. The change in the roughness of the sample during the incubation period is almost similar with the both setups, whereas the roughness post incubation period is not quite similar to each other [17]. Each of them has their own pros and cons which are briefly listed in Table 1.

Table 1 Comparison of RET setups [18]

	Whirling Arm	**Pulsating Jet**
Erosion Area	Large, Uncontrolled	Small, Controlled
Droplet size	Controlled	Controlled
Droplet Shape	Uncontrolled	Controlled
Sample Shape	Fixed	Flexible
Reproducibility	Good	Good
Costs	High	Low

As the sample is stationary, it is easy to install the piezoelectric sensors or strain gauges and the measurements are comparatively subjected to less noise. A pulsating jet erosion test setup requires low investment and the results are reproducible, should make it a go to solution for the testing of rain erosion performance.

2.5 Parameters effecting the erosion

To understand the initiation or propagation of the erosion, a good understanding of the parameters affecting the erosion is required. In this sub chapter a literature study on the important parameters which can affect the erosion behaviour is provided.

2.5.1 Impact Velocity

The impact velocity is one of the main parameters that influences the erosion. It depends on several factors such as the length of the blade, rotational speed and the terminal velocity of the incoming rain drops. The actual impact velocity is a combination of rotational speed of the blade and the terminal velocity of the rain droplet.

The terminal velocity of the rain droplet is dependent on the climatic conditions, mass and size of the drop. The maximum terminal velocity of a rain droplet through stagnant air is around 9.2 m/s [19]. For an example, when the turbine blade rotates with a tip speed of 90 m/s and the terminal velocity of the rain droplet is 8 m/s, fully entrained in a wind of 20 m/s blowing horizontally, the impact velocity between rain droplet and blade at various positions can be seen in Figure 11 [20].

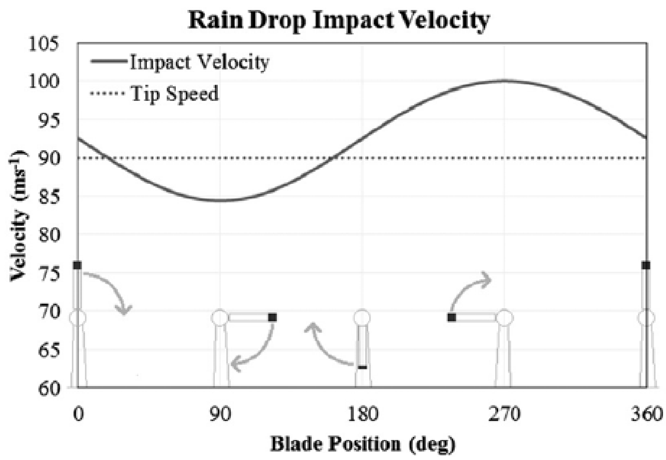

Figure 11 Rain droplet impact velocity at various blade positions [20]

This states that the effect of terminal velocity is very less on the impact velocity. The current turbine blades are being operated at a high tip speeds exceeding 100 m/s which results in higher impact velocities.

2.5.2 Angle of Impact

As the leading edge of the wind turbine is a curved surface, the angle of impact of a rain droplet varies from the stagnation point to the laminar separation point. Therefore, the parameter angle of impact has its significance in the rate of erosion. Whenever the droplet hits the specimen at an angle, the horizontal component of the impact velocity is responsible for the majority of the erosion, whereas the vertical component is responsible for the surface area covered by the droplet. This can be well explained by the concept of vectors. From Figure 12, if θ is the angle of impact, then $\theta = tan^{-1}\left(\frac{V_y}{V_x}\right)$. From this relation it can be understood that the impact velocity decreases with the increase in the angle of impact.

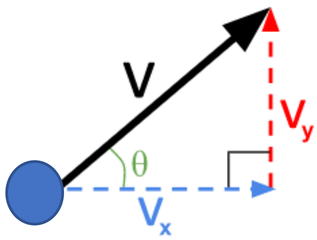

Figure 12 Velocity components of a droplet

Studies state that the increase in the angle of impact corresponds to the increase in the volume loss of material, also the highest erosion rate is found at an impact angle of 90^0 with the vertical which is perpendicular to the blade [21, 22].

2.5.3 Droplet size and shape

The size and shape of the rain droplet also determines the rate of erosion. It has been found that the large drops can cause erosion at lower velocities than those required for small droplets as the hammer pressure created on the surface by the large drops is higher than that of the small droplets [15]. The higher radius of curvature of a water droplet can be a significant reason for intensive irrespective of the mass of the same water droplet [23].

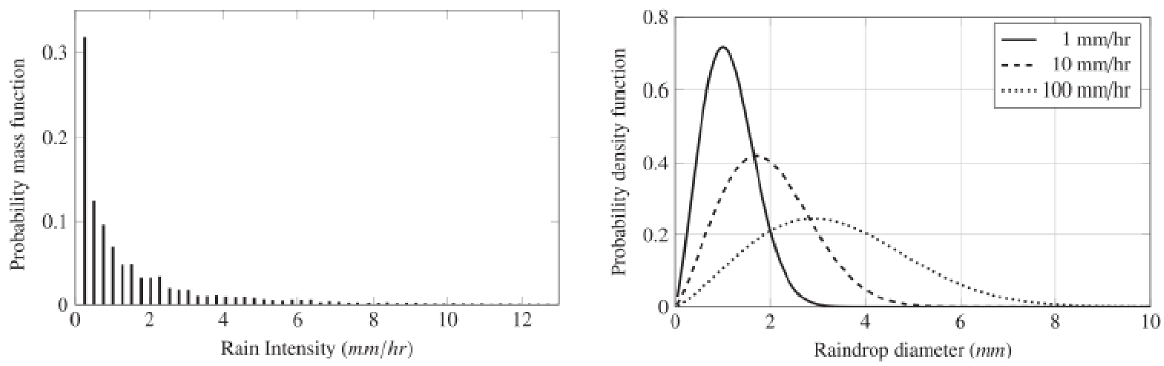

Figure 13 Rain data of New Bedford between 1992 and 2000 [12]

Raindrops are considered to have a perfect sphere shape, but it is only in the case of droplets with diameter of less than 2 mm. The shape of the droplet is highly dependent on its diameter. A raindrop of up to 2 mm diameter is in spherical shape, whereas it is semi-oblate for droplets with diameter between 2 mm and 5 mm. Based on Figure 13, it can be inferred that the size of the most occurring rain droplets is of less than 2 mm in diameter.

2.5.4 Impact Frequency

The frequency of impacts is an important parameter as the erosion is a result of multiple impacts. Whenever there is a second impact on the specimen in very short interval of time, there is a high possibility of positive interferences between the waves which can create additional damage. Therefore, the time before the introduced stress is vanished and impact frequency are important parameters that must be considered [24].

In one of the previous researches to control the impact frequency a rotating disc of 20 Hz has been used which consist of two orifices on opposite sides of the disk in order to create the water jet slugs. This results in an impact frequency of 20 Hz, which corresponds to a rainfall of 25 mm/h [17].

2.5.5 Wet Surface

During the water droplet impacts there is a high chance of the water droplets to be trapped in the pits or form a layer over the specimen which might reduce the erosion damage. When the incoming droplets hit the wet surface of the sample, the liquid layer deforms and the specimen will not experience the same pressure as of a dry specimen. Therefore, the presence of a water layer on the surface of the material can result in misleading observations. A water removal system should be implemented in the rain erosion test setup to study the erosion behaviour [12].

2.5.6 Loads acting on a wind turbine blade

There are many loads acting on the wind turbine blade, out of those the aerodynamic loads and gravity are the primary loads on the wind turbine blade. The aerodynamic loads acting on the blade are the reason for the fatigue damage. The drag forces are the major concern when the turbine blade is stationary, whereas the lift forces create the aerodynamic loadings while the turbine is operating. The combination of these loads creates stresses in the blade that ultimately lead to fatigue failure [25].

The leading edge of the wind turbine blade is under continuous tensile loading case which results in additional strains in the material used as the protection for the leading-edge erosion. These additional strains might influence the way the stress waves interact with the protective material.

2.6 Research Questions

More knowledge about the failure mechanisms and the important parameters effecting the erosion is required in order to understand the damage occurrence and its propagation in the materials used for leading edge protection. The following are the research questions formulated for this research project.

- **How does the erosion occur and develop in the materials used for LEP?**
- **Is there any effect of water layer present on the sample on the rain erosion?**
- **What is the influence of additional strains on the rain erosion of leading-edge protection for a wind turbine blade?**

To answer the first question of the research, a detailed plan of experiments is required in order to identify the occurrence of the erosion and its progression as the number of impacts on a sample increase. This research objective is also helpful to understand the length of incubation of the materials used for the leading-edge protection.

In order to answer the next research question, a water removal system is to be modelled and installed to the rain erosion test setup which will be helpful to study the effect of water layer on the rain erosion performance of the material.

The final research question is involved with few theoretical calculations to find out the strains acting on a wind turbine blade. In the later stages of the research these strains will be incorporated into the LEP material by modelling a tensile pull system which will be installed to the rain erosion setup to analyse the influence of additional strains in the material on the rain erosion.

3 Experimental Methodology

In order to answer the first question of the research, a rain erosion test facility is required to conduct few sets of experiments which will be helpful to study the occurrence and progression of the rain erosion. A pulsating Jet erosion test (PJET) setup was readily available at a facility in Hengelo, The Netherlands provided by University of Twente which was designed and built by ir. Douwe Jan Pel under the supervision of ir. Nick Hoksbergen and dr. Ismet Baran.

Figure 14 Model of the PJET setup [12]

The model of the pulsating jet erosion test setup which can be seen in Figure 14 allows the user to adjust the four most important rain erosion parameters namely the size of the raindrop, impact velocity, impact frequency and angle of impact. The size of the raindrop is determined by the nozzle size and the geometry of the rotating disc. The important factors which vary the impact velocity are the pump pressure and the diameter of the nozzle. The pump installed in the PJET setup was a Speck 22 plunger pump. The maximum velocity that can be attained by the setup is 186.85 m/s with a 1.2 mm nozzle, at a pump pressure of 180 bar [12]. The most important parameters of the PJET setup including their ranges are listed in Table 2.

Table 2 PJET setup's important parameters and their ranges [12]

Parameter	Range
Diameter of the nozzle	0.6 - 1.6 mm
Impact velocity	0 – 186.85 m/s
Impact frequency	20 - 200 Hz
Angle of impact	90 – 10.7^0

The angle of impact can be adjusted by rotating the hinges of the fixture, whereas the impact frequency can be altered by using different slotted rotating discs as shown in Figure 15. A stepper motor (Ezi-Servo Plus-R 56L) with a nominal torque output of 1.5 Nm is used to rotate the disc at a velocity of 600 rpm [12].

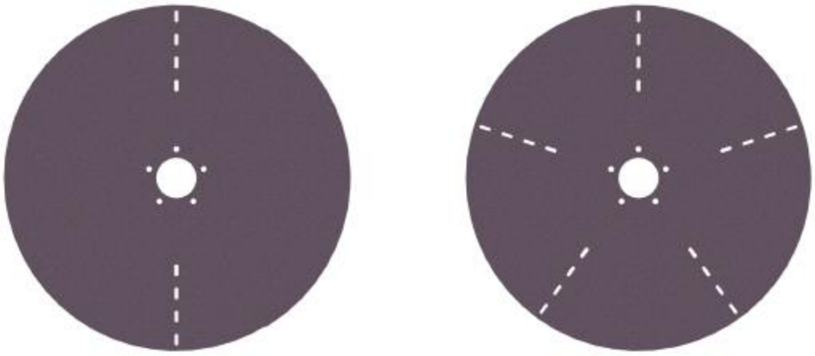

Figure 15 Rotating disc design, Left: 20 Hz, Right: 50 Hz [12]

In order to answer the second question of the research which is regarding the effect of the water layer on the erosion performance of the specimens, an air blowing system was installed on the setup to blow away the water layer which is formed on the specimens during the impacts of the water jets. An Abac Pole Position 241 air compressor with a flat air nozzle which has a maximum working pressure of 8 bar was installed. The compressor has an air tank of 24 L with a capacity of 240 L/min [12]. Depending on the experimental requirement, the air blowing system can be easily installed or uninstalled from the setup. As shown in Figure 16, the flat air nozzle was mounted on the fixture clamp so that the compressed air flows 10 mm away from the impact location of the water droplet. This design can minimize the risk of the water jets being influenced by the flow of air during the impacts.

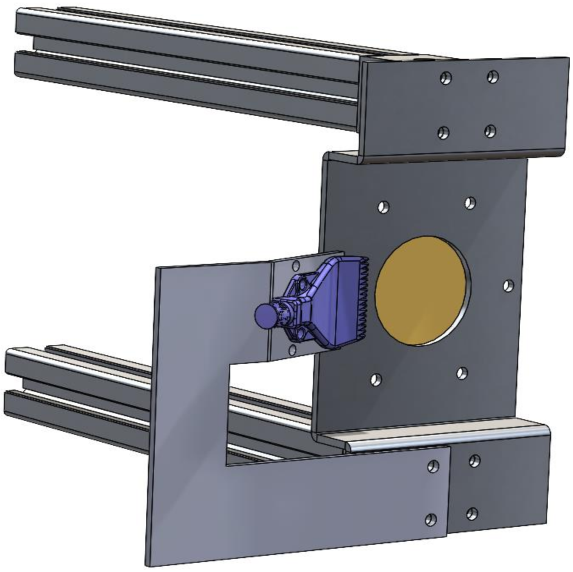

Figure 16 Flat air nozzle mounted on the fixture clamp

3.1 Preliminary Experiments

In this research, Acrylonitrile Butadiene Styrene (ABS) is the main focus for the material to be used as the leading-edge protection of a wind turbine blade. To study the surface of the impacted specimens a Keyence VK9710 laser scanning confocal microscope was chosen which is available at the microscopy lab of University of Twente.

As the margin of error with the location of droplet impact is in millimetres, the sample cannot be placed at the exact same position so that the location of impact does not alter. Also, the PJET setup and the microscope were not in a single facility. This increases the total time spent on the experiments and microscopy. Hence, it was decided to perform each set of impacts on a different sample i.e., after performing 25.000 impacts, a new sample is placed in the setup to impact the sample for 50.000 times to obtain the results for 50.000 impacts. This is a time-consuming process especially when the research is aimed to study the behaviour at higher number of impacts ranging over 1 million impacts.

Rain erosion of a material is a result of repeated impact of rain droplets. Therefore, to study the occurrence and progression of the erosion the number of impacts on the sample was varied ranging from 25.000 to 500.000 impacts which is shown in Table 3. The parameters such as the nozzle diameter, impact velocity, impact frequency and angle of impact were kept constant throughout the entire set of experiments. A pump pressure of 160 bars with an output nozzle diameter of 1.0 mm was used to achieve a water stream with a velocity of approximately 175 m/s which is then cut into jet slugs by using a rotating disc which rotates at a speed of 600 rpm. These jet slugs further travel to hit the specimen at an impact angle of 90^0 with the vertical at a frequency of 200 Hz.

Table 3 Preliminary experiments without air blower

Material	Nozzle Diameter (mm)	Impact Velocity (m/s)	Impact Frequency (Hz)	Angle of Impact (w.r.t vertical)	Number of Impacts
Acrylonitrile Butadiene Styrene (ABS)	1.0	175	200	90^0	25.000
					50.000
					100.000
					150.000
					200.000
					300.000
					400.000
					460.000
					500.000

To study the influence of the water layer, a number of experiments were conducted varying from 25.000 to 400.000 impacts which is shown in Table 4. Similar to that of the preliminary experiments, the parameters such as the nozzle diameter, impact velocity, impact frequency and angle of impact were kept constant. In addition to the above-mentioned parameters, a constant pressure of 2 bar compressed air was used to remove the water layer on the specimen.

Table 4 Preliminary experiments with air blower

Material	Nozzle Diameter (mm)	Impact Velocity (m/s)	Impact Frequency (Hz)	Angle of Impact (w.r.t vertical)	Pressure of Compressed Air (bar)	Number of Impacts
Acrylonitrile Butadiene Styrene (ABS)	1.0	175	200	90^0	2	25.000
						50.000
						100.000
						150.000
						200.000
						300.000
						400.000

All the samples were taken to the microscopy lab at the University of Twente, to analyse the surface of the samples and identify the erosion behaviour of the material. The next chapter discusses the characterization of the tools and techniques used to understand the rain erosion behaviour of the material.

4 Methodology for analysis

To understand the erosion behaviour of the material, the impacted samples have been studied under VK9710 Keyence confocal microscope using 10x lens and overview images which were assembled using several pictures made out of 10x lens. Using the VK Analyzer software the height maps of the surface of the specimens have been extracted and the data obtained has been analysed using MATLAB.

The output of the confocal microscopy results in various surface roughness parameters such as maximum pit depth (Sv), maximum Peak height (Sp), maximum height (Sz), skewness (Ssk), arithmetical mean height (Sa), Kurtosis (Sku), root mean square height (Sq) with each of them having their own purpose. The VK Analyzer software can also be used to determine the results of the parameters but the filtering value used by the software to reduce the noise is unknown. Therefore, a MATLAB code was prepared in order to evaluate these parameters including the volume loss of the specimens. In this chapter the significance of these surface roughness parameters has been explained and a detailed view on the above-mentioned parameter's reliability while working with the rain erosion specimens will be provided.

4.1 Roughness Parameters and their significance

Sp is the parameter which gives the height of the highest peak in the given region [26]. While obtaining the height, a mean plane will be determined and the maximum height among all the peaks over the mean plane can be obtained. Therefore, the value obtained by this parameter is based on a single pixel. The pictorial representation of this parameter has been described in Figure 17. Sp is an areal extension of Rp.

$$S_p = \max\,(Z(x,y))$$

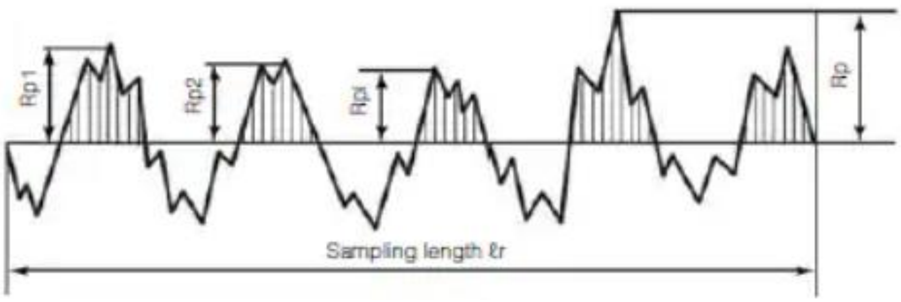

Figure 17 An example of maximum profile peak height of a line [26]

Sv is the parameter which evaluates the depth of the lowest pit in the given region [26]. In order to obtain the lowest pit, a mean plane will be considered and the maximum depth among all the pits below the mean plane can be obtained. Similar to that of Sp, Sv is also dependant on a single pixel. Such dependence can lead to undesirable effects as the height maps collected from the microscope consists of considerable noise. The pictorial representation of this parameter has been described in Figure 18. Sv is an areal extension of Rv.

$$S_v = |\min(Z(x,y))|$$

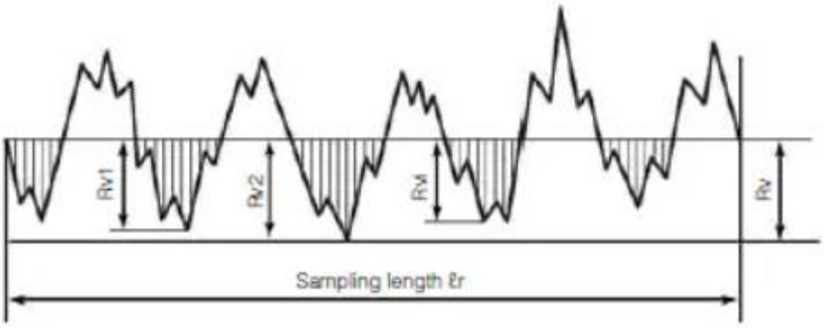

Figure 18 An example of maximum profile valley depth of a line [26]

There are certain limitations while using the above-mentioned parameters. The microscopy images which are made of using 10x lens are not representative when there are large craters, as the complete crater cannot be fitted into a single image, which results in contradicting data points. The overview images which are assembled using 10x images can be used to analyse these parameters as the whole size of the craters can be fitted into a single image. Figure 19 represents the scenario of 10x zoom images and overview images.

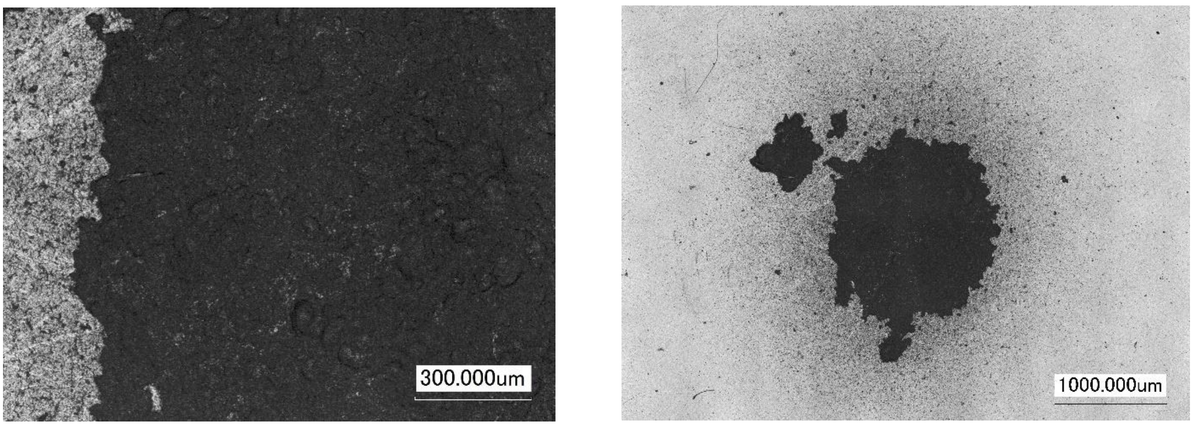

Figure 19 Left: 10x zoom image; Right: Overview image of 400.000 times impacted ABS Sample with air blower

There are few setbacks while working with these parameters, one of those is the initial scratches on the surface of the sample. Due to the manufacturing defects in the samples few unwanted pits and scratches occurs on the surface of the sample which leads to anomalies in the results, as these scratches on the surface are deep enough to draw into wrong conclusions. The highlighted part in the Figure 20 shows the potential defects in the sample.

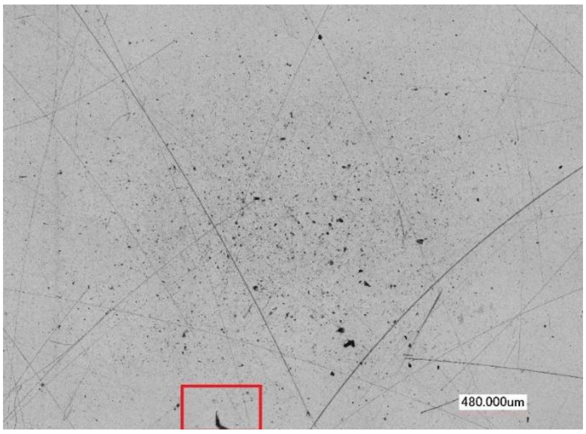

Figure 20 Defects in the ABS 50.000 times impacted sample

Using the VK Analyser software the location of the maximum peak value was obtained and it lies outside of the erosion region which clearly states that these defects have influence on the results. In Figure 21, it can be seen that the maximum peak height in the bottom section of specimen which is outside of the erosion region is 113.75 µm which is higher than the 66.35 µm of maximum peak height from the section which contains the eroded part. To avoid such instances the images obtained through microscopy were trimmed so that these defects were not included in the images.

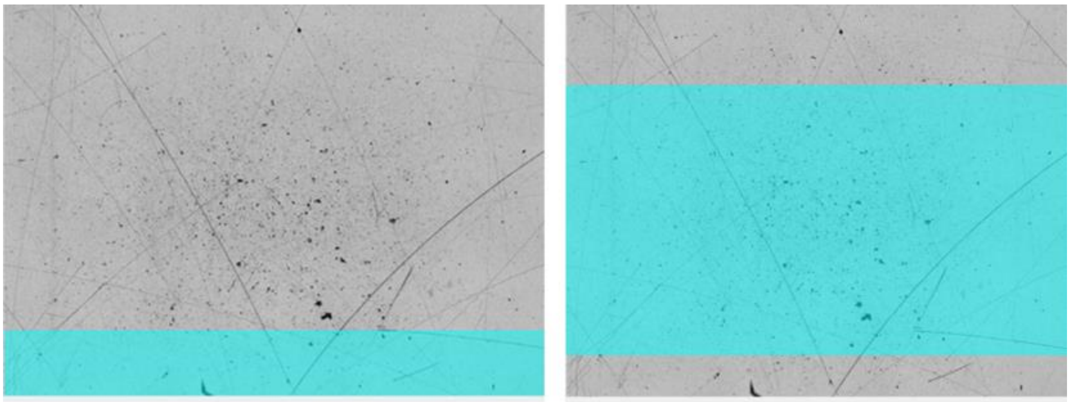

Figure 21 Surface roughness parameters of various sections of a specimen

The trimmed images have significant role to play when there are defects in the sample, but it is not possible to trim the images when there are defects lying within the eroded part of the sample. Therefore, it is difficult to analyse the results when there are defects in the sample. Figure 22 shows the influence of the trimmed images when there are anomalies present in the sample.

To compute the results all these parameters take the mean plane into consideration as a reference. The average of all the heights on the surface will be calculated to obtain the mean plane. Using these parameters, the depth of the craters or the height of the peaks can only be studied until there is a big crater, further measurements cannot be taken into account because the mean plane in the heavily eroded samples is already way below compared to that of the less eroded samples.

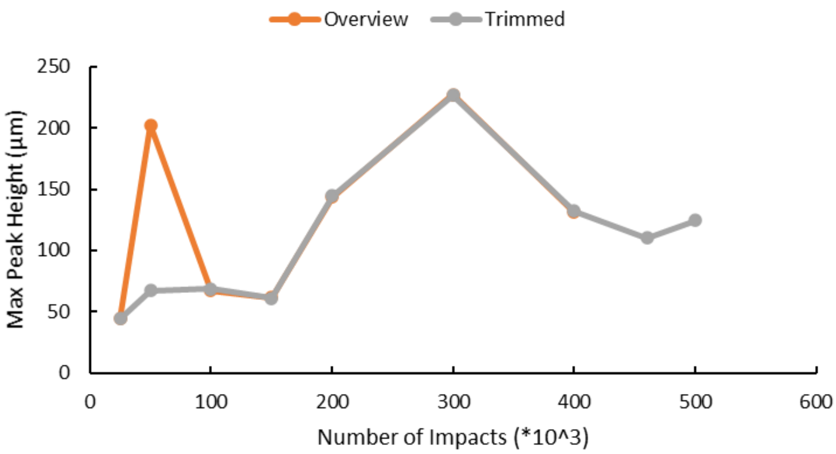

Figure 22 Comparison of Overview and Trimmed images for Sp

In the Figure 22, a dip in the maximum peak height from the 400.000 impacts can be observed, which should not be the case as the peak height was expected to increase with the higher amounts of erosion. This can be well explained by the mean plane effect as the large craters on the surface resulting in the low mean plane compared to that of other samples. The large craters covering the majority of the images can be seen in the Figure 23.

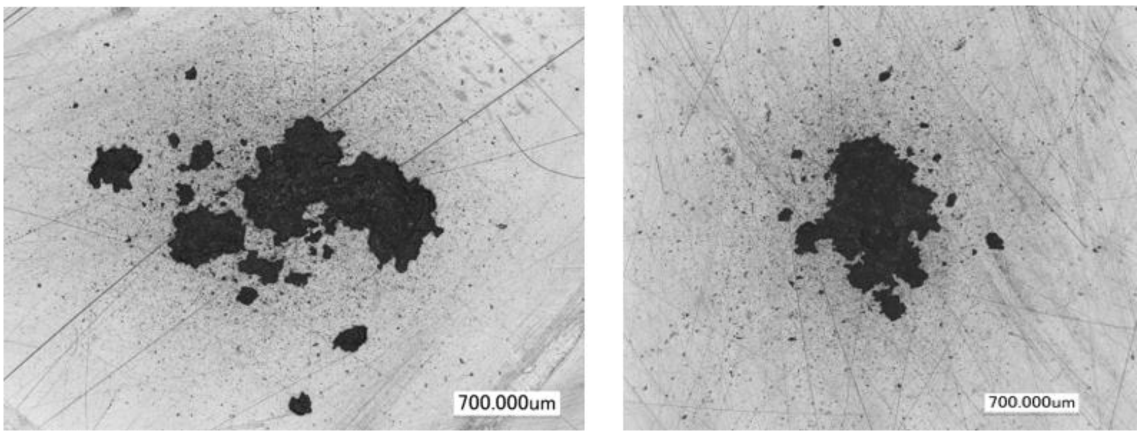

Figure 23 Left: ABS sample with 400.000 impacts; Right: ABS sample with 460.000 impacts

Due to the lack of a constant reference plane, the mean reference plane keeps on changing from one sample to the other, the parameters Sv and Sp are not suitable to study the erosion behaviour.

The parameter Sz represents the distance between highest peak and lowest pit on the surface [26]. In simple terms Sz can be understood as sum of the parameters Sp and Sv. The pictorial representation of this parameter has been described in Figure 24. Sz is an areal extension of Rz.

$$S_z = S_p + S_v$$

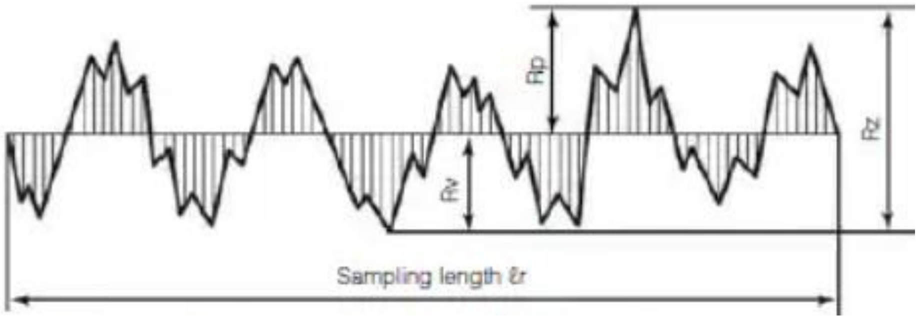

Figure 24 An example of maximum profile height of a line [26]

This parameter could be useful as there is no effect of mean plane on the outcome of the results. But the Sz parameter is highly susceptible to noise present in the results which often leads to wrong conclusions. Figure 25 shows the signs of noise in the data obtained from the confocal microscope. The parameters such as Sz, Sp and Sv which are highly dependent on values of a single pixel are prone to bad outcomes due to the influence of noise in the readings. Therefore, these parameters are not suitable to study the erosion behaviour.

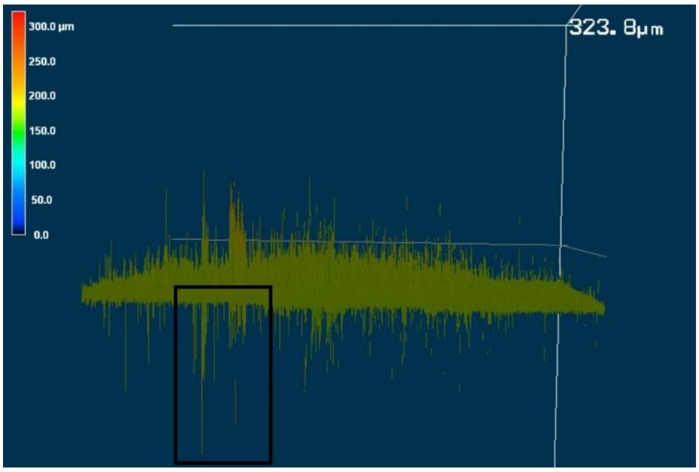

Figure 25 Height map of ABS 200.000 impacts

The parameter Sa is defined as the arithmetic mean of all the absolute heights on a surface with respect to the mean plane of the surface [26]. This parameter is the three-dimensional extension of line roughness parameter Ra. The pictorial representation of Sa can be seen in the Figure 26.

$$S_a = \frac{1}{A}\iint_A |Z(x,y)|dxdy$$

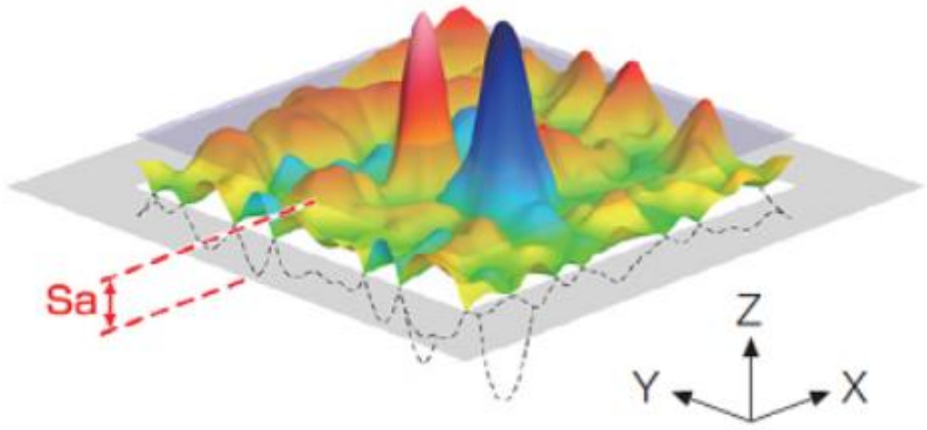

Figure 26 An example of arithmetic mean height of a surface [27]

Sq is the parameter which represents the root mean square value of ordinate values within the definition area as shown in the Figure 27. It is equivalent to the standard deviation of heights [26]. Similar to that of Sa, Sq also represents the vertical height of the surface. Sq is an areal extension of Rq.

$$S_q = \sqrt{\frac{1}{A}\iint_A |Z^2(x,y)|dxdy}$$

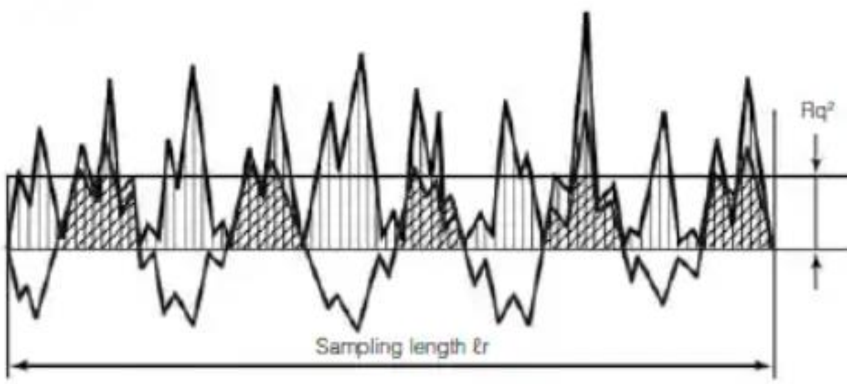

Figure 27 An example of root mean square deviation of a line [26]

The parameters Sa and Sq are useful only to depict the relative height of the surfaces but do not provide any information regarding the formation of pits and the emergence of craters. It is possible to have similar Sa or Sq for surfaces with different roughness profiles as seen in the Figure 28. However, to calculate the parameters Sa and Sq a mean plane is taken into consideration and the height of each ordinate is calculated from the mean plane. As few irregularities were observed in the results of previously mentioned parameters where mean plane plays a major role, therefore Sa and Sq parameters are not considered to study the erosion behaviour.

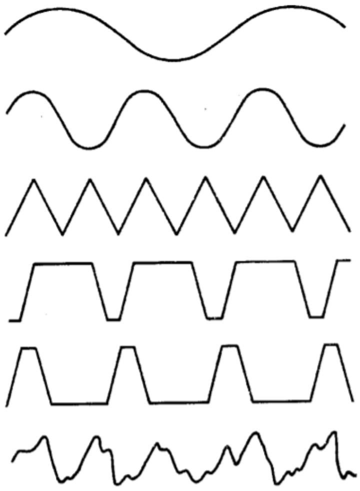

Figure 28 Various Surface profiles with similar Ra [28]

Kurtosis is the next parameter to consider, Sku (kurtosis) is the measure of the sharpness of the distribution. It is the three-dimensional expansion of the line roughness parameter Rku which is defined as the quotient of the mean quadrative value of the absolute values of all the heights and the fourth power of Rq [27]. The kurtosis surface roughness parameter is a dimensionless quantity without a unit.

$$S_{ku} = \frac{1}{S_q^4}\left\{\sqrt{\frac{1}{A}\iint_A |Z^4(x,y)|dxdy}\right\}$$

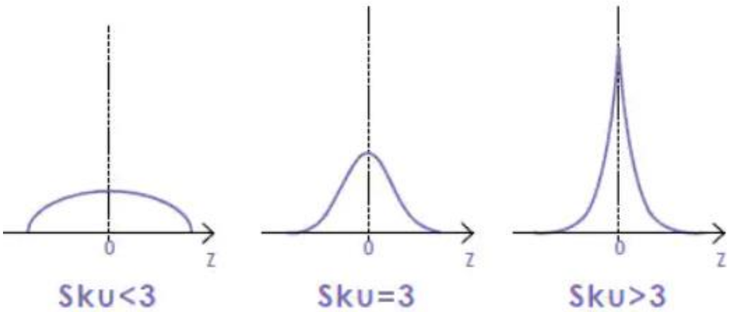

Figure 29 Symmetrical distribution with different kurtosis [26]

Roughness profiles with kurtosis higher than 3 indicate that the height distribution is sharp with high peaks and the Sku value of less than 3 states that the surface has rounded peaks with craters or pits [29]. If the surface heights are normally distributed then the kurtosis value is equal to 3, which could be seen in Figure 29.

In order to study the characteristics of a distribution, a representative surface is essential. The overview images are not quite representative as the size of each overview images is not constant for all the microscopy images. In this scenario using single images made out of 10x lens at the centre of the eroded surface could be the best fit. Therefore, kurtosis is only valid until there is a huge crater, as the 10x images are not representative anymore when there is a huge crater.

The final surface roughness parameter is skewness (Ssk) which represents the degree of symmetry of the height distribution of a roughness profile. It is the three-dimensional expansion of the line roughness parameter Rsk which is defined as the quotient of the cube of the mean of the absolute values of all the heights and the cube of Rq [27]. The skewness surface roughness parameter is a dimensionless quantity without a unit.

$$S_{sk} = \frac{1}{S_q^3}\left\{\sqrt{\frac{1}{A}\iint_A |Z^3(x,y)|dxdy}\right\}$$

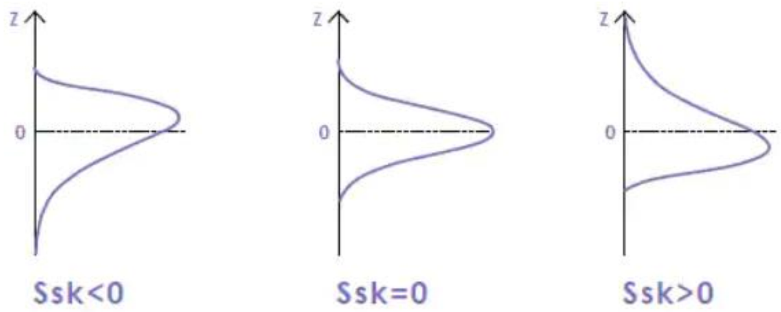

Figure 30 Probability density functions for random distributions with different skewness [26]

As seen in the Figure 30, the roughness profiles with positive skewness indicate that the surface consists of peaks and the intensity of pitting is very low whereas the surfaces with greater number of pits or with craters have a negative skewness. The zero skewness explains that the peaks and pits co-exist on the surface i.e., the height distribution is symmetrical about the mean plane [29].

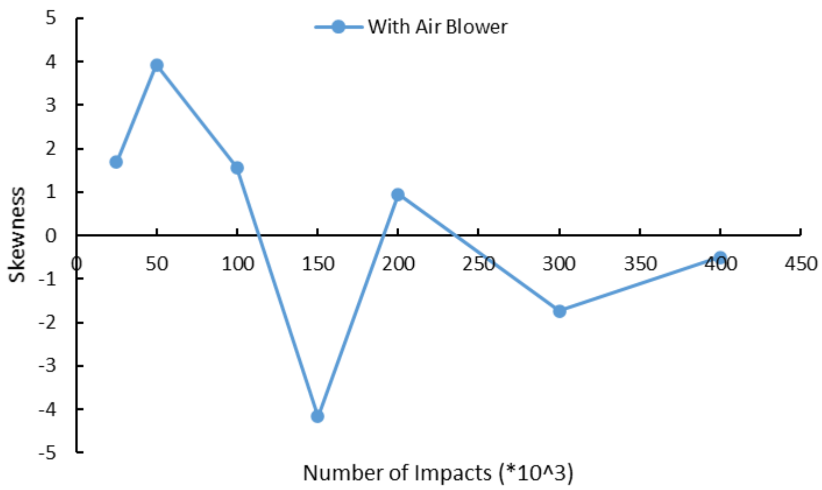

Figure 31 Skewness of the impacted ABS samples obtained from 10x images

As the number of impacts on a sample increases the amount of erosion also gradually increases resulting in the formation of pits and craters. Skewness is the parameter which tells about the intensity of the pits which can be used to understand the extent of erosion before the formation of craters. Similar to Kurtosis, Skewness is also only valid until there is a huge crater, as the 10x images are not representative anymore when there is a huge crater.

The outliers in the Figure 31 do not effectively prove that the parameter does not hold during every situation. Defects in the sample such as initial surface roughness or unknown errors during the experiments could be the reason for such anomalies.

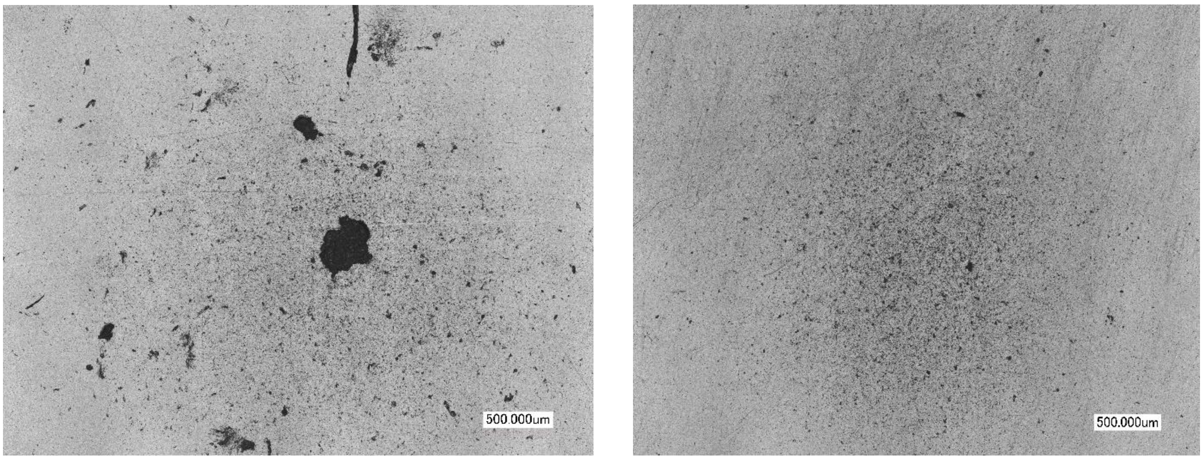

Figure 32 Left: ABS sample with 150.000 impacts; Right: ABS sample with 200.000 impacts

From the Figure 32 it can be assumed that the sample used for 150.000 impacts has initial manufacturing defects which might lead to higher erosion and formation of craters whereas the other sample has intensified pits on surface without any formation of craters. This can be clearly inferred by Figure 31 as 150.000 impacts has lower skewness than the 200.000 times impacted sample. Therefore, it can be concluded that skewness is the parameter to understand the erosion behaviour until the formation of large craters.

4.2 Volume Loss Algorithm

Volume loss describes the amount of material lost on the surface due to erosion. It is useful in understanding the level of erosion on the samples. The stitched images by using 10x lens which gives the overview of the complete erosion region are the best source of data to study the volume loss. The higher the amount of volume loss, the severe is the erosion damage on the specimens. In order to determine volume loss of a sample, the height profile of the eroded region will be needed to be extracted by the confocal microscope.

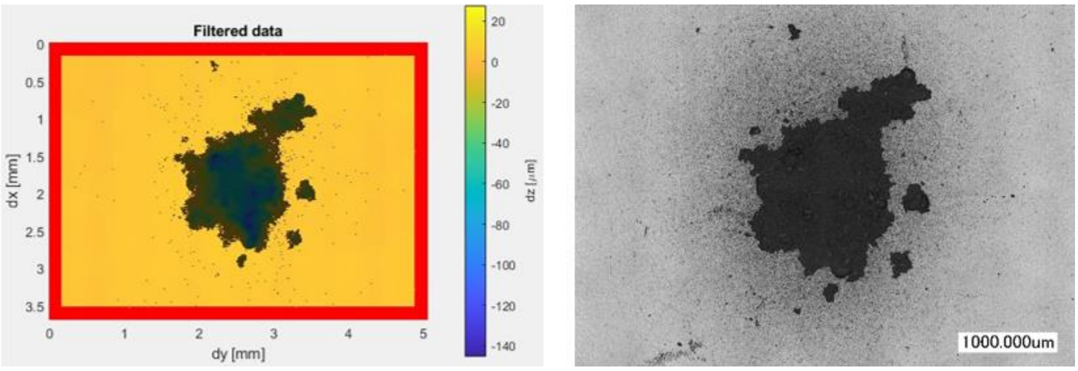

(a) (b)

Figure 33 (a) Example of reference plane in volume loss algorithm; (b) Laser intensity image

As shown in the Figure 33(a) a reference surface was fitted with respect to the undamaged material on the boundaries of the image. It is very important to have erosion free boundaries for the stitched images, so that the obtained volume loss results are reliable. The total deviation of the height profile with respect to the fitted reference surface will be taken as the volume loss in the distance to mean method. Same as roughness parameters, the volume loss algorithm can also be affected by the noise or erroneous values.

When a reference surface is fitted at the boundary of the image, it is not guaranteed that it is perfect plane surface without any peaks or pits. This could lead to bad results from volume loss algorithm Therefore, the standard deviation of all the points lying within the reference surface is considered, which creates a new plane of reference with the help of standard deviation values. This new plane can be slightly lower than the previous reference surface. The volume loss is computed by considering the points which are below this new reference plane but computing their distance to the original reference surface fitted at the boundaries of the image [30]. As seen in Figure 33(a) the dark regions are considered for the calculation of volume loss which is almost similar to the crater that can be seen in Figure 33(b). Therefore, this method can reduce any potential erroneous values or noise. It is highly recommended to have an erosion free surface on the edges of the image while computing volume loss.

5 Experimental Repeatability

In the previous chapter, the tools and parameters which will be used to analyse the results of the rain erosion tests were described. Volume loss algorithm was applied to the confocal microscopic data of the preliminary experiments, Figure 34 shows the obtained results:

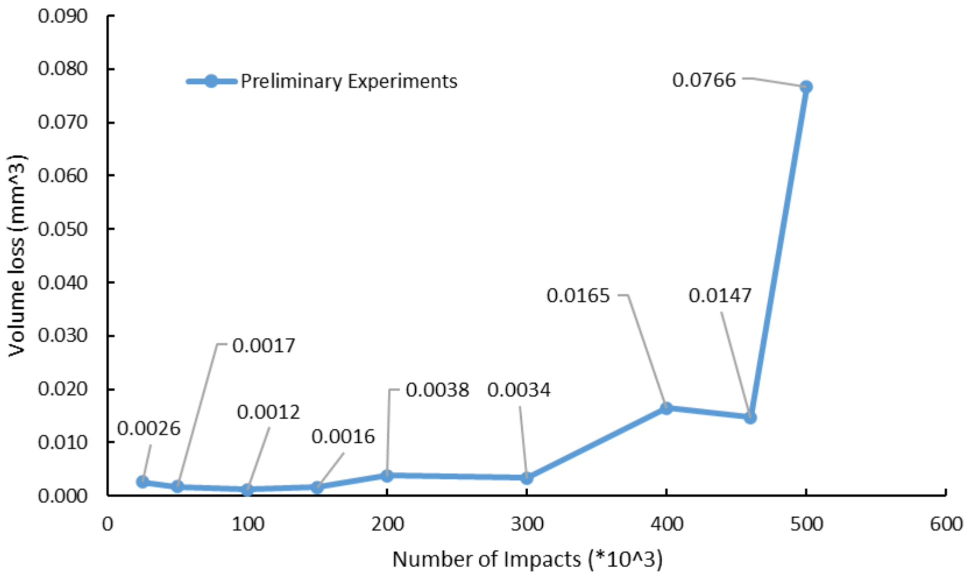

Figure 34 Volume loss vs Number of impacts for preliminary experiments

The volume loss on the surface of the material was expected to increase with increase in number of impacts. Therefore, it was expected to see a steadily increasing graph, but the results obtained were contrary to the expectations. Although in the initial stages i.e., till 300.000 impacts, the amount of volume loss is considerably low to discuss regarding the deviations, the volume loss obtained at 460.000 impacts is 10% lower than the volume loss obtained at 400.000 impacts which is definitely an outlier. A critical review on the experimental approach is required to find out any possible ambiguities and provide possible alternatives to increase the quality of the research.

5.1 Tests for repeatability

Outliers are one of the common issues in any sort of scientific research. The possible reasons for outliers could be (i) errors in microscopic data, (ii) initial surface roughness of specimens (iii) experimental procedure or (iv) manufacturing defects. It is important to conduct a critical review on the experimental methodology to find out the possible reason for outliers. To validate the repeatability of the obtained results, it was decided to repeat the tests stated in the preliminary experiments chapter.

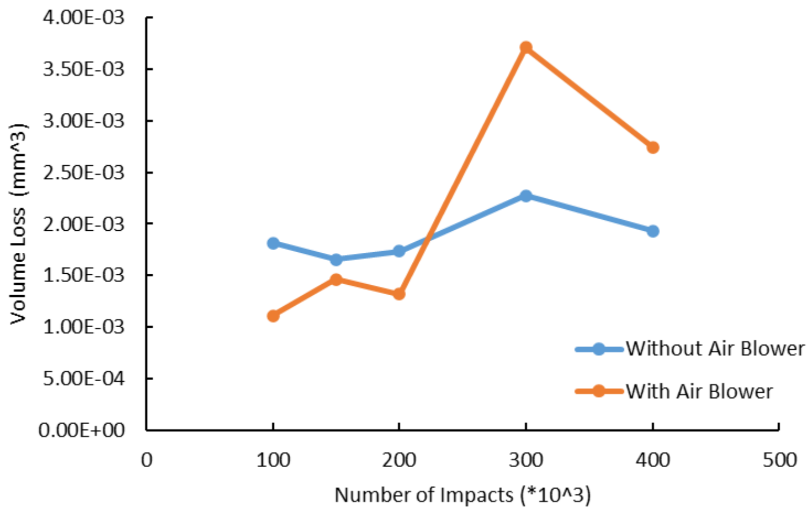

Figure 35 Volume loss vs Number of impacts for second iteration

The results of the second iteration can be seen in Figure 35. The volume loss obtained during the second iteration is very low compared to that of the preliminary experiments. Also, the volume loss obtained could be seen fluctuating even with the increase in number of impacts. The reasons for this abnormal behaviour were investigated and it was found that the pulsation damper used in the PJET setup to control the pressure and flow of the water jet was broken. Therefore, the malfunctioning pulsation damper could not hold the required pressure and flow, which led to the erroneous results.

5.2 Silicone Approach

Due to the COVID-19 regulations, it took over three months to repair the broken setup. This created problems with the experimental scheduling to continue with the research, as it consumes a lot of time to repeat the whole set of experiments, which is not affordable. At this stage, to reduce the time spent on the experimental work a new experimental approach was proposed where silicone material was used.

In the new silicone imprint approach for the experimental work, the silicone material used in the food industry for making moulds was proposed to make the imprints of the surface of the material. Until this stage of the research, each 'number of impacts' test was performed on a different sample, but from hereafter it was decided to perform all the impacts test on a single sample by taking an imprint using silicone after the required number of impacts on the sample. For example, if an experimental plan to perform 200.000, 400.000 and 600.000 impacts was proposed, then all the impacts can be done on the same sample without removing it from the fixture clamp, reducing the risk of misalignment when placing the sample back and more importantly reducing the total number of impacts from 1.200.000 (200.000+400.000+600.000) to 600.000 impacts saving nearly 60 minutes of testing. The silicone material is used to take the imprint of the surface after the desired number of impacts, in this example it is after 200.000 and 400.000 impacts.

By following this approach, all the experiments can be done on a single sample which reduces the time spent on experiments. The other important advantage of this approach is that the reference surface of all the results will be the same which gives better results while performing a qualitative analysis. The first silicone imprint was made on an already existing sample of ABS, which is used for the rain erosion experiment to understand the potential of this silicone imprint approach. The silicone imprints and the sample were analysed under the Keyence VK9710 laser scanning confocal microscope.

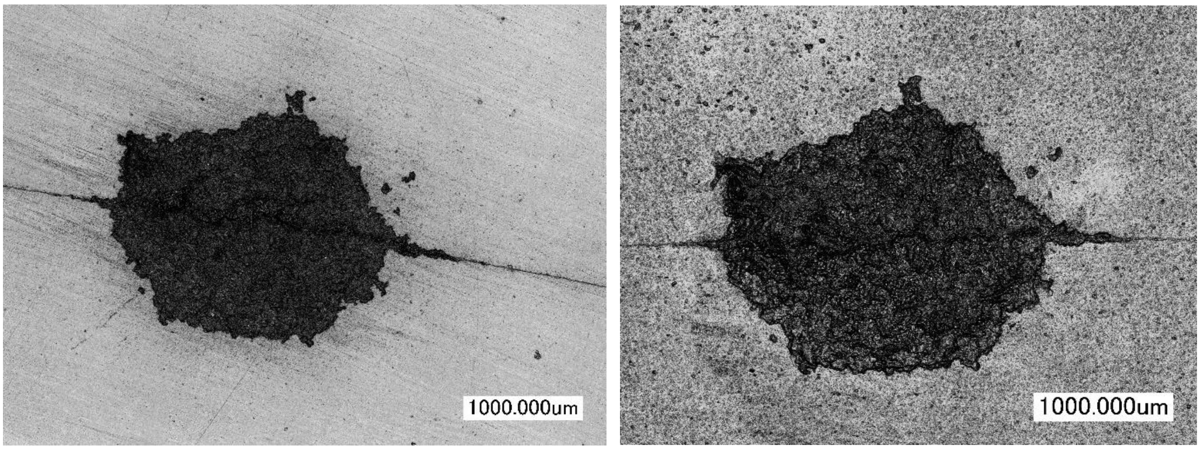

Figure 36 Laser intensity images Left: ABS sample; Right: Silicone imprint

As it can be seen from Figure 36 the silicone material has shown a great potential in making fruitful imprints of the surface of the sample. The silicone imprint of the crater resembles to that of the crater on the ABS sample. The volume loss on the ABS sample and the silicone imprint was found to be 0.130mm^3 and 0.129mm^3 respectively. From the volume loss readings, it can be understood that the silicone material was able to capture the entirety of the crater in its imprint.

The disadvantage of these silicone materials used for preparing the moulds is that it takes one hour of time to completely cure. The time taken to make the imprint is very much higher than the time taken to complete the test, which is not desirable. For an example, if a test set of 25.000, 50.000 and 75.000 impacts is decided to perform, then the time taken to take the imprints of the surface of these specimens will be around 3 hours, whereas the elapsed time of three experiments itself is around 14 minutes. These slow curing silicones can be handy to reduce the time spent on the tests when the range of impacts is very high i.e., over 400.000 impacts

Therefore, a new type of fast curing silicone material "Struers replifix-2" was selected to decrease the time for curing the silicone the material. A set of tests need to be conducted to validate that the silicone imprints can be used to continue with the research. Table 5 shows the list of experiments conducted to validate the silicone approach.

Table 5 List of Experiments to validate silicone approach

Material	Nozzle Diameter (mm)	Impact Velocity (m/s)	Impact Frequency (Hz)	Angle of Impact (w.r.t vertical)	Number of Impacts
Acrylonitrile Butadiene Styrene (ABS)	1.0	175	200	90^0	800.000
					1000.000
					1200.000
					1400.000
Gelcoats	1.0	175	200	90^0	100.000
					200.000
					300.000
					400.000
Polycarbonate	1.0	175	200	90^0	600.000

The silicone imprints and the sample were analysed under the Keyence VK9710 laser scanning confocal microscope. As seen in Figure 37, the laser intensity image of the silicone imprint and the gelcoat sample resembles each other. By looking at these images, it can be understood that the silicone imprints have succeeded to make the overview image of the erosion area. The volume loss on the gelcoats sample and the "Struers replifix-2" silicone imprint was found to be $0.108mm^3$ and $0.153mm^3$ respectively, such a difference in the volume loss figures was not acceptable.

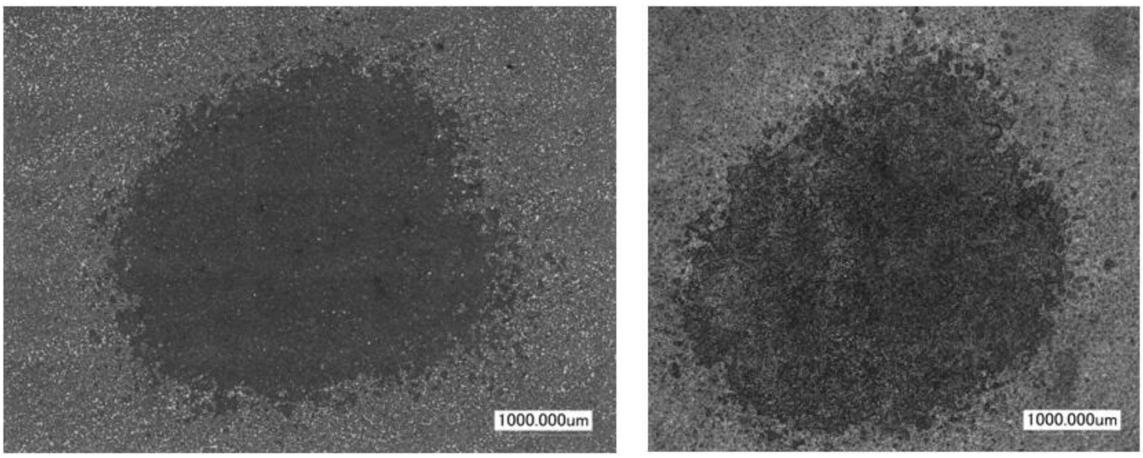

Figure 37 Laser Intensity images Left: Gelcoats 400.000 sample; Right: "Struers replifix-2" silicone Imprint 400.000

To understand the reason for the difference in the volume loss, the height profiles extracted from the microscope were verified. Unfortunately, the height profiles of the "Struers replifix-2" silicone imprints obtained by the microscope were not useful, as the readings consist of heavy noise which is the reason for the variation in the volume loss values of the gelcoats sample and its imprint. This makes it difficult to analyse the extent of erosion on the surface of the samples. Figure 38 shows the heavy noise in the extracted height profiles.

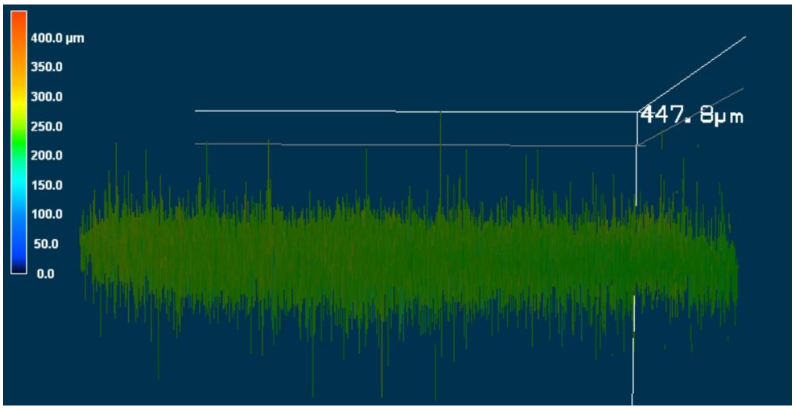

Figure 38 Height maps of a "Struers replifix-2" silicone imprint

Although different microscope settings and a Keyence VHX 7000 digital microscope were used, the noise in the height map profiles could not be eliminated. The reason for the noisy readings was unknown. Moreover, in few imprints there were micro voids such as in Figure 39, showing that air could be trapped during the curing of silicones or a possible high shrinkage of silicone locally, thereby questioning the reliability of this approach. Various techniques such as applying heat and uniform pressure while taking the imprints were used but none of those could provide required results.

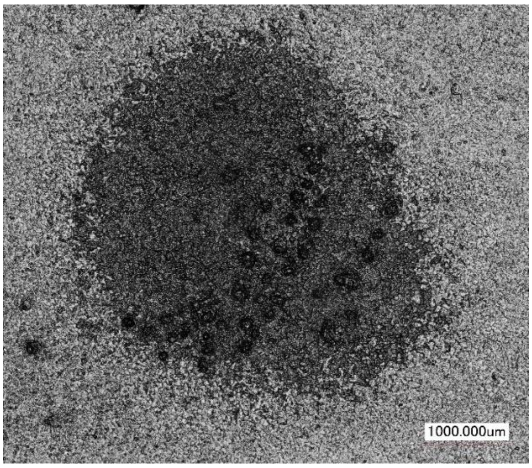

Figure 39 "Struers replifix-2" silicone imprints with micro voids

Therefore, considering all the drawbacks with this approach such as slow curing time, micro voids and noise data, it was decided to withdraw from this approach for further research.

5.3 Change in ideology

The silicone approach was intended to decrease the amount of time spent on the experimental work; however, it did not work as planned. Hence, a different approach was required to continue with the experimental work. So, the only possible option to reduce the duration of experiments is by altering the fixture clamp of the PJET setup. As seen in Figure 40, the fixture clamp consists of six screws to tighten the clamp. During the preliminary and second iteration experiments the sample positioning was as shown in the Figure 40(a), which makes it difficult to reposition the sample at the same position once it is removed out of the fixture. Due to this drawback, different samples were used

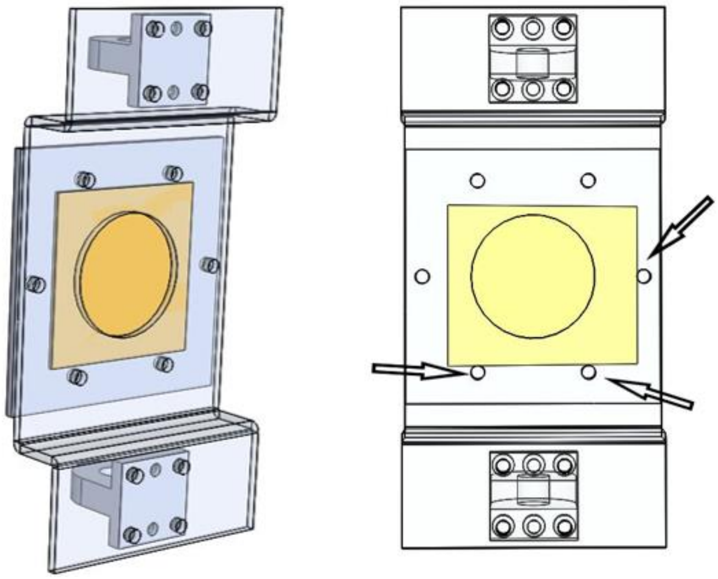

(a) (b)

Figure 40 (a) Old positioning of sample, 40(b) New positioning of sample

Whereas in the new positioning of the sample which is shown in Figure 40(b), the sample was placed over the two screws on the bottom and pushing the sample on to the screw on the right side of the clamp will allow the sample to be placed in its previous position with very minimum tolerance. By this procedure, the sample can be removed from the setup whenever it is required and placed it back in the setup to continue with the next set of experiments.

Advantages of this method are:

- Various number of impact tests can be conducted on a single sample, which allows one reference surface for all the experiments.
- The elapsed time of each test reduces, which allows to reach higher number of impacts such as 1.8million to 2 million.

Disadvantages of this method are:

- As the microscope and PJET setup were not located in a single facility, it takes more time to complete the entire experimental procedure including microscopy.
- When the sample is removed from the fixture clamp, the alignment of the sample for the further experiments at the exact same position is not guaranteed.

In order to answer this issue, the experimental plan could be divided into two parts, conducting on two different samples. The lower number of impacts can be performed on the first sample and the higher number of impacts on the other sample. In this way the issue with reference surface which is predominant at lower number of impacts can also be solved even while using different samples.

By implementing this approach further set of experiments were planned as seen in Table 6. The impact tests under 200.000 impacts were neglected as the volume loss at those impacts was found out to be very minimum based on the preliminary experiments.

Table 6 Experimental plan implementing new approach

Material	Sample Number	Nozzle Diameter (mm)	Impact Velocity (m/s)	Impact Frequency (Hz)	Angle of Impact (w.r.t vertical)	Pressure of compressed air (bar)	Number of Impacts
Acrylonitrile Butadiene Styrene (ABS)	1	1.0	175	200	90^0	N.A.	200.000
							400.000
							600.000
	2	1.0	175	200	90^0	N.A.	800.000
							1.000.000
							1.200.000
	3	1.0	175	200	90^0	2	200.000
							400.000
							600.000
	4	1.0	175	200	90^0	2	800.000
							1.000.000
							1.200.000

In the next chapter a detailed analysis of the results of these experiments will be provided.

6 Result Analysis

In this chapter, the results of the rain erosion experiments are analysed both qualitatively and quantitatively. For the quantitative approach, surface roughness parameters and volume loss algorithm based on MATLAB codes were used, whereas for qualitative approach the laser intensity images of the laser scanning confocal microscopy were utilized.

6.1 Occurrence and development of erosion

The volume loss of the ABS material which is to be used for the leading edge of the wind turbine blades has been evaluated using the volume loss algorithm. The volume loss curve of the material seen in Figure 41 is similar to that of the stages of erosion curve learnt during the literature review chapter. From the preliminary experiments until 200.000 impacts, it was found that the volume loss on the surface of the material is 0.0038 mm^3 which is negligible. This particular stage can be explained as the incubation stage of the material where the material loss is negligible. During this stage the surface of the material gets rough due to the formation of pits when hit by the water droplets.

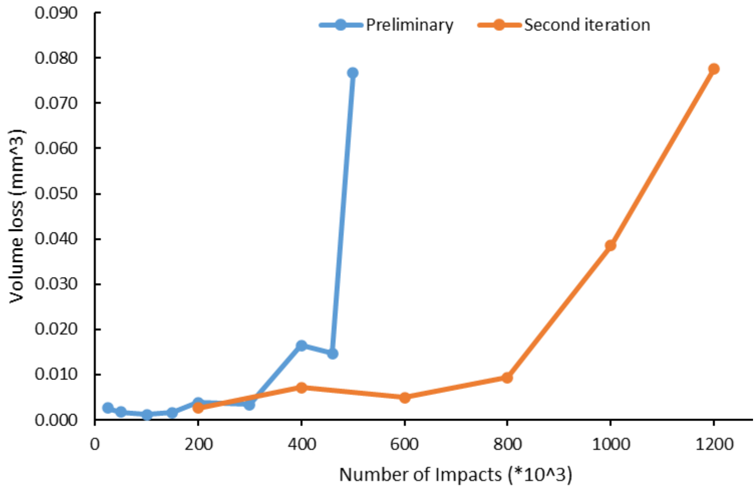

Figure 41 Volume loss vs Number of impacts curve for without air blower scenario

From the 200.000 to 600.000 impacts, with a range of 400.000 impacts the volume loss on the surface of the material slightly increased from 0.0026 mm^3 to 0.0049 mm^3. The ABS material is still in the phase of incubation at the 600.000 impacts as the volume loss obtained at this stage is still considerably very low, whereas at 800.000 impacts the volume loss on the sample incremented by 90% reaching 0.0094 mm^3. This sudden increase in the volume loss can be adjudged as the end of the incubation phase and transition of the material into the early stages of acceleration phase. During this phase the intensified pits occurred at the end of incubation phase start developing into mini craters by merging with one another.

From the volume loss curve in Figure 41 it can be identified that the acceleration period is very short in the ABS material as the volume loss at 1.000.000 impacts is 0.03858 mm^3 which is four times higher than that of the volume loss obtained at 800.000 impacts. A volume loss of 0.07772 mm^3 has been observed at 1.200.000 impacts which is double the volume loss obtained at the 1.000.000 impacts. Therefore, this stage can be classified as the maximum erosion rate of the ABS material. The overall aim is to prevent the erosion damage on the material. Therefore, the end of incubation point is the most important focus of this research for the practical application of ABS material as the leading-edge protection of the wind turbine blades. To understand further erosion development, more experiments are needed to be conducted to identify the duration of the maximum erosion stage and the kick start of the deceleration phase of volume loss.

While comparing the two sets of experimental results, it was understood that the volume loss at 500.000 impacts for preliminary experiments was equivalent to that of 1.200.000 impacts of second iteration. This difference in the volume loss is very huge, this needs to be investigated as the parameters used to conduct the experiments were same. As there is one year of time gap between the two set of experiments, aging factor of the material was assumed to be the reason for this abnormal behaviour. Therefore, the preliminary experiments were not considered for the analysis of the results. Further studies in the related field are required to understand the effect of aging in ABS material. In the case of second iteration experiments, the higher volume loss obtained at 400.000 impacts than that of at 600.000 impacts is due to the noisy readings from the confocal microscope. This reading can be neglected, as both the tests were conducted on a single sample.

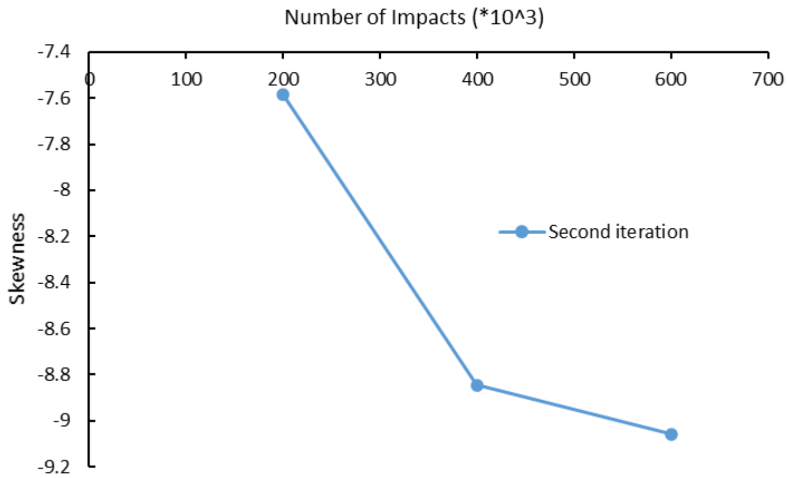

Figure 42 Skewness vs Number of impacts

The skewness (Ssk), surface roughness parameter is used to determine the intensity of pits on the surface of the material. However, this can be used only until there is a big crater on the surface. The negative skewness values in the Figure 42 indicates that the surface of the material consists of pits and increasing negative values show that the intensity of the pits is increasing with the increase in number of impacts.

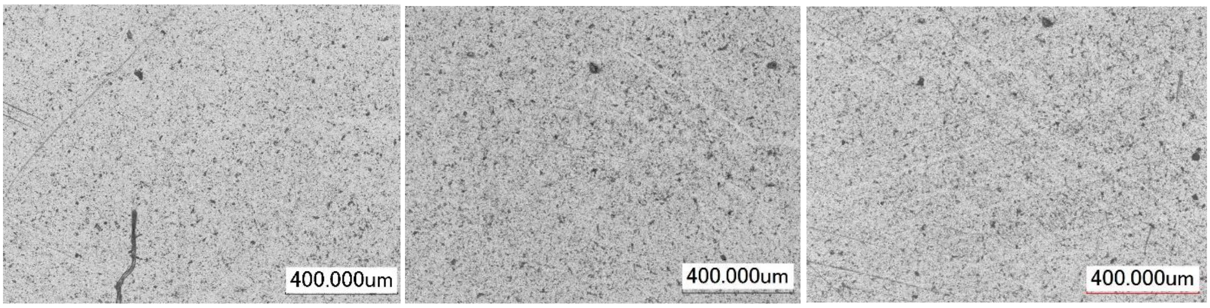

200.000 400.000 600.000

Figure 43 Laser intensity images by 10x zoom confocal microscope lens

Figure 43 shows the 10x zoom images of the surface of the sample focused at the centre of the erosion damage. Here, the transition of pitting intensity from 200.000 to 600.000 impacts can be seen. As the number of pits on the surface increases, the surface roughness of the material increases. When compared to a smooth surface, a highly rough surface is prone to lateral jetting which increases the intensity of erosion by combining the pits into craters. In Figure 44 the progression of rain erosion of ABS material from 200.000 impacts to 1.200.000 impacts can be seen.

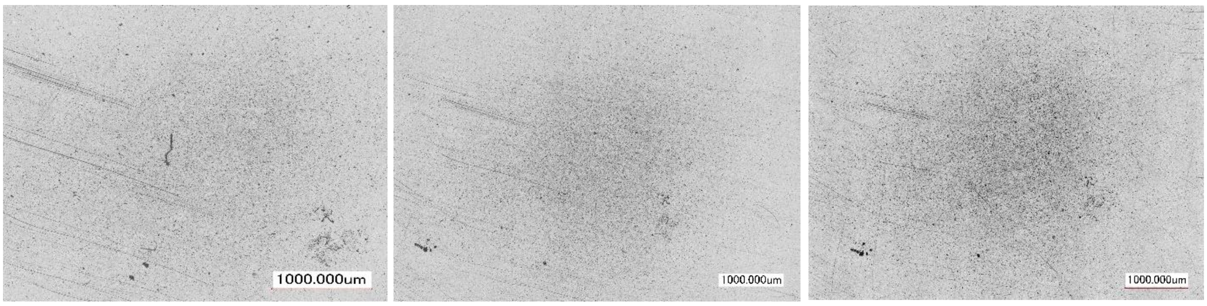

200.000 400.000 600.000

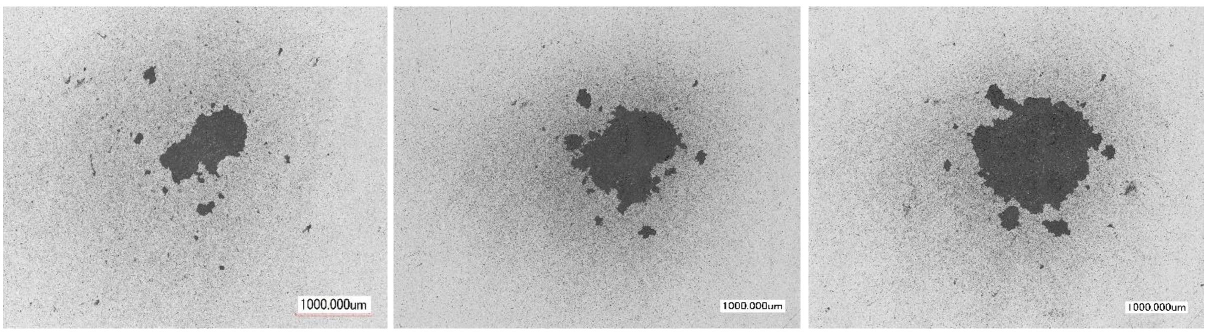

800.000 1.000.000 1.200.000

Figure 44 Laser intensity images of overview of erosion

At 600.000 impacts, intensified pitting on the surface of the material can be seen from Figure 44, which later resulted in the formation of crater at 800.000 impacts by the increased effect of lateral jetting which ended the incubation phase of the material. At 1.000.000 impacts, the size of the crater started growing rapidly with emergence of small craters in the vicinity due to the intensified pitting. At this stage, the maximum depth of the crater is around 135 µm, which was 100 µm at 800.000 impacts. This shows that the erosion not only spreads on the surface of the material, but also into the material. After the 1.200.000 impacts, the small craters previously lying around the big crater also merged into the crater to further increase the level of the erosion. The formation of new pits around the craters seems to be inevitable due to the continuous lateral jetting process. These pits grow into craters and merge into the existing big crater. The maximum depth of the crater at 1.200.00 impacts is 205 µm, revealing that the craters are rapidly growing deeper as well.

6.2 Effect of water layer

In the above subchapter, it was identified that the aging of material can have an effect in the rain erosion performance of the material. Therefore, the results of the preliminary experiments with water layer removal system were not mentioned as they were not relevant to the new set of experiments. In this subchapter, the effect of water layer on the rain erosion performance of the materials will be analysed by comparing the scenarios of the experiments conducted by using an air blower to remove the water layer to that of the experiments where no such technique was used.

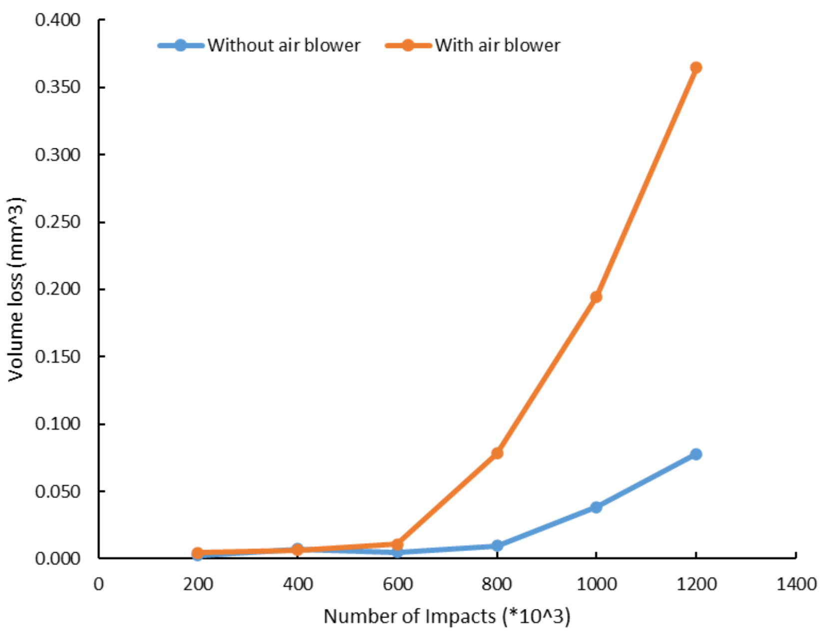

Figure 45 Volume loss comparison of without and with air blower

The comparison of volume loss on the surface of the ABS material in both the cases can be seen in Figure 45. At every stage, the volume loss is found to be higher when the water layer is removed on the surface of the material. In the initial stages, i.e., till 400.000 impacts the amount of material lost is negligible in both the cases, but, at 600.000 impacts the volume loss while using the air blower is double that of the volume loss at 600.000 impacts without using the air blower.

This transition at 600.000 impacts can be understood as the material has passed its incubation phase and the early commencement of acceleration phase of erosion in the case of air blower compared to that of the without air blower. Thereafter, the rate of material loss increased rapidly. A volume loss of 0.07835 mm^3 was recorded at 800.000 impacts which is equivalent to the volume loss at 1.200.000 impacts in the case of without air blower. By these volume loss values, it can be understood that the ABS material has a short phase of acceleration. The volume loss at 1.000.000 and 1.200.000 impacts was 0.195 mm^3 and 0.365 mm^3 respectively, which is five times higher than that of the respective cases of the without air blower condition. The ABS material is still assumed to be in the phase of maximum erosion state even after a material loss of 0.365 mm^3, as the deceleration of the rate of erosion could not be identified after 1.200.000 impacts.

The progression of rain erosion of ABS material when the water layer is removed can be seen in Figure 46. The comparison between Figure 44 and Figure 46 can give an insight regarding the intensity of pitting and formation of craters on the surface of the ABS material.

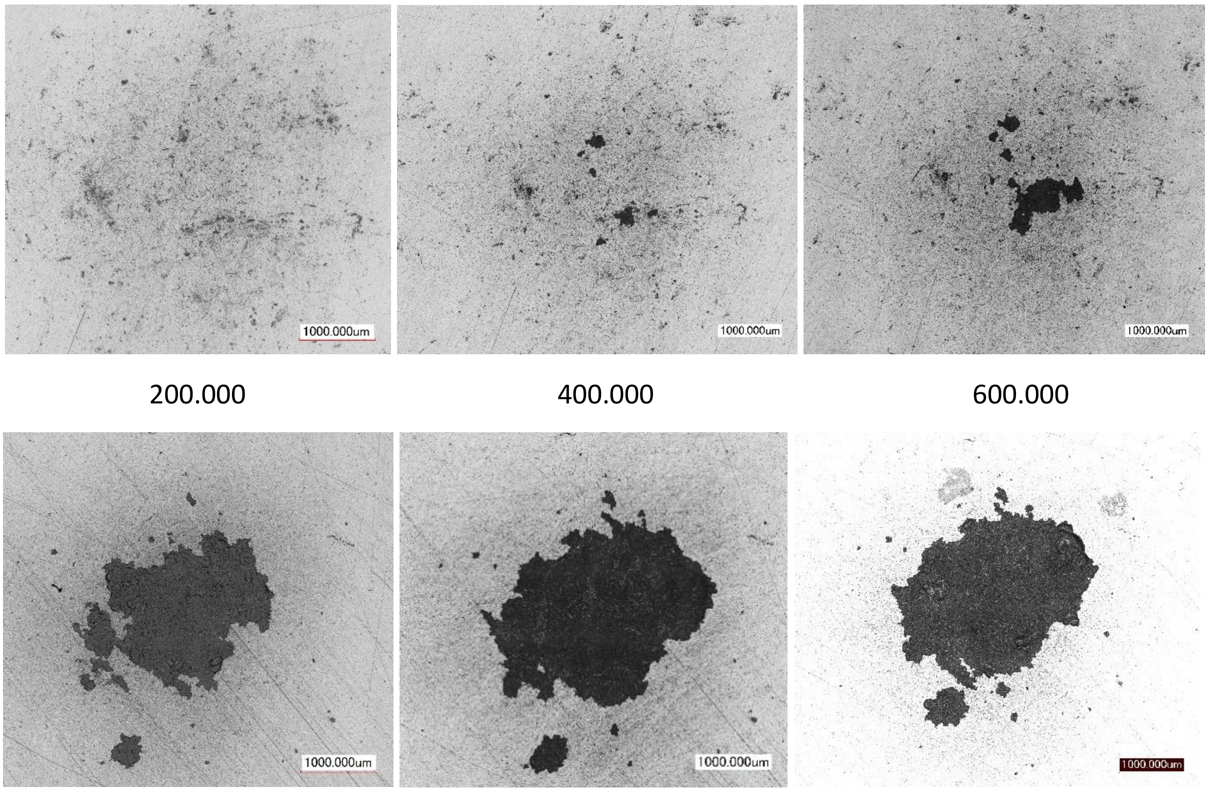

800.000 1.000.000 1.200.000

Figure 46 Laser intensity images of overview of erosion without water layer

In Figure 46, at 200.000 impacts, the level of pitting intensity is higher than that of in Figure 44. It can be seen from Figure 48 and Figure 42 that the value of skewness at 200.000 impacts when an air blower is used was -9.4, which is higher than that of the without air blower case where the skewness at 200.000 impacts is -7.6. Also, few pits already started forming into minute craters. At 400.000 impacts, the intensified pits started growing into small craters which later at 600.000 impacts merged together leading to the formation of a big crater which clarifies that intensified pitting is the major reason for the formation and growth of craters. Further at 800.000 impacts, the formation of a huge crater can be seen in Figure 46, which depicts that the material entered its maximum rate of erosion state. As the number of impacts increased, the erosion damage intensified with increase in the maximum depth of the craters. The maximum depth of the craters at 1.000.000 and 1.200.000 is 270 µm and 290 µm respectively, which does not justify the huge difference in the volume loss of the material at these impacts.

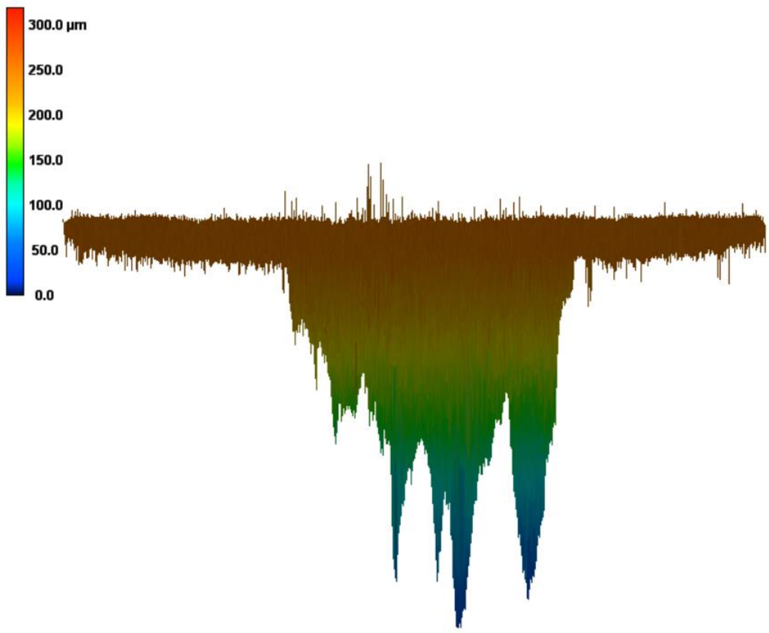

Figure 47 Height map of ABS 1.200.000 impacts with air blower

Figure 47 shows that the maximum depth of the crater should not be considered at higher volume loss of the material to describe the level of erosion as there can be more than one deepest point of the crater, which do not contribute to the maximum depth of the crater, but plays a huge part in the volume loss values. The maximum depth of the crater depends on a single pixel, whereas the volume loss algorithm considers an area to compute the volume loss of the sample. Therefore, this particular scenario proves that volume loss is a dependable parameter to work on with the result analysis of the rain erosion experiments when compared to the maximum depth of the craters.

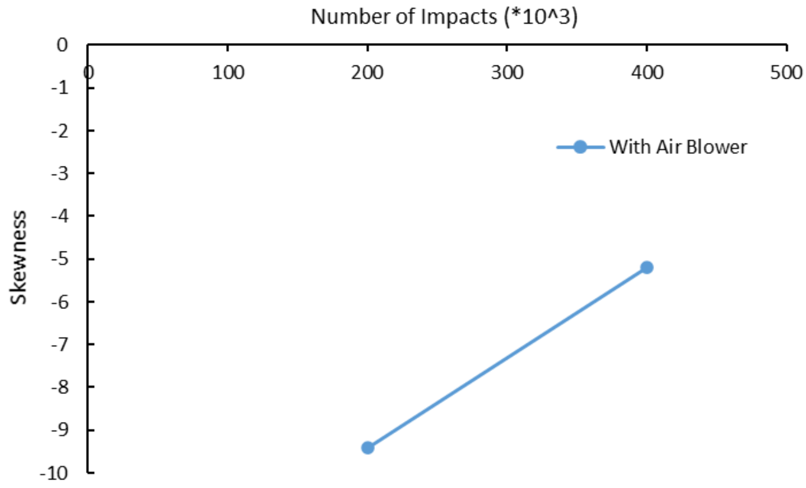

Figure 48 Skewness vs Number of impacts

The skewness at 400.000 impacts is higher than that of the skewness at 200.000 impacts. This can be explained by using Figure 49 that shows a crater in the 10x zoom image which is used to study the skewness parameter. The skewness parameter is only valid until there is a crater on the surface of the material, because the skewness parameter is not representative anymore when there is a crater in the 10x zoom image. This means that the skewness parameter holds well to understand the intensity of pitting on the surface of the material.

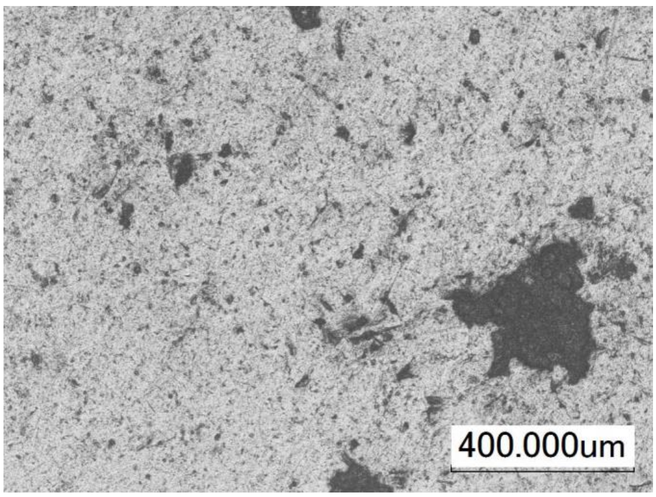

Figure 49 Laser intensity 10x image of ABS 400.000 impacts with air blower

From the above-mentioned analysis, it can be inferred that the water layer created on the surface of the material, due to the water droplet impacts has a significant effect on the rain erosion performance of the material. This can be predominantly observed when the material passes its incubation phase, because by the end of the incubation the surface of the material is covered with intensified pits, any further impacts can increase the rate of volume loss of the material. When there is the presence of a water layer, the rough peaks on the surface of material are protected by the water layer from erosion due to the incoming impacts and the lateral jetting of the droplets. This results in lower volume loss on the surface of the specimen. During the operation of the wind turbine, either the heavy wind blows away the water layer on the surface of the blade or the water layer does not exist due to the centrifugal force acting on the blade. Therefore, the presence of a water layer in the real time working conditions of a wind turbine blade is not possible, which results in higher volume loss of the material. Therefore, the results of the tests with the water layer removal system should be compared with the tests performed on whirling arm setup to understand the importance of the water layer.

7 Effect of Strain

The leading edge of the wind turbine blade is under continuous tensile loading case which results in additional strains in the material used as the protection for the leading-edge erosion. When a rain droplet hits the surface of the material it creates a compressional shock wave which propagates through the material. When there is an existing strain in the material, the stress created by the compressional shock waves resulted from the impacts of the droplet sums up with the initial strain in the material, which can result in changes in the erosion behaviour of the protective material. Therefore, in this chapter a study on the effect of additional strains in the material on the rain erosion performance of the ABS material was conducted.

The stress acting on the leading edge of the wind turbine blade is due majorly due to the edgewise bending moment, centrifugal force and the own weight of the blade. Sandia 100m all-glass baseline wind turbine (SNL100-00) was taken as reference to calculate the amount of stress acting on the leading edge of the blade [31]. From Figure 50 it can be understood that the stress due to centrifugal force and weight of the blade decreases from root to the tip of the blade. The stress due to edgewise bending moment depends on the cross-section of the air foil. From Figure 51 it can be inferred that the maximum stress due to edgewise bending is obtained at 25% of the blade fraction.

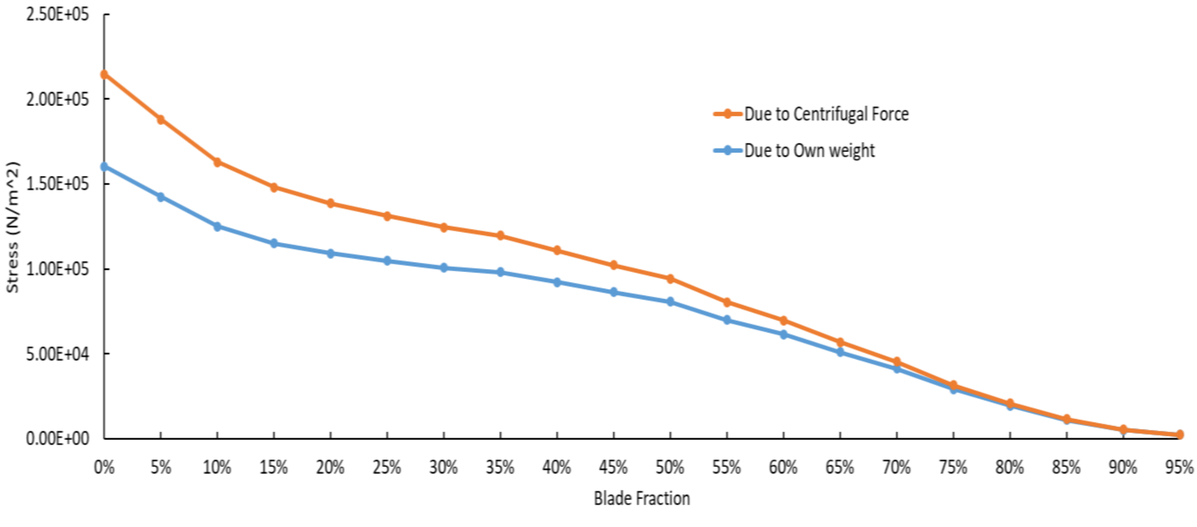

Figure 50 Stress due to centrifugal force and weight of the blade vs Blade fraction

The maximum stress on the leading edge of the wind turbine is the resultant of these three major stresses which was calculated to be 8.84 MPa which was vastly due to the edgewise bending moments of the wind turbine. In this research, Acrylonitrile Butadiene Styrene (ABS) is the material of interest to study the rain erosion performance of the material when utilized as the leading-edge protection of the wind turbine blades. The young's modulus of ABS is 2.50 GPa. Therefore, the strain in the ABS material when used as the leading-edge protection material of the wind turbine blades was computed to be 3.53 micro-strains which is 0.353%.

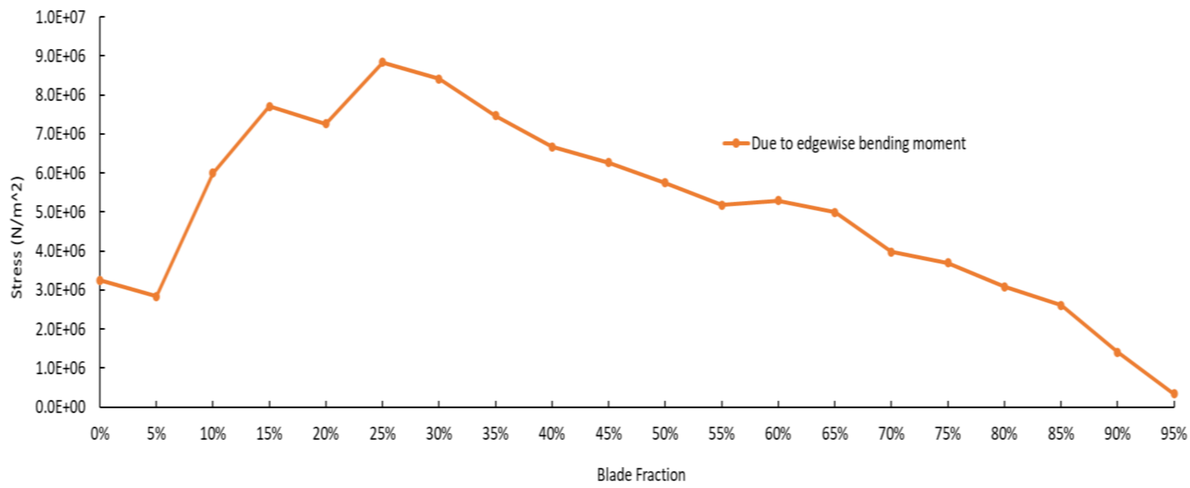

Figure 51 Stress due to edgewise bending moment vs Blade fraction

Figure 52 shows a SOLIDWORKS model of the tensile clamp which will be added to the pulsating jet erosion setup to induce additional strains to the ABS material while impacting with the water droplets. The tensile clamp consists of two lead screws on either side of the fixtures which can be rotated to impart the horizontal tensile loading on the material. The machine threads of M10*1.0 will be used for the lead screws. If a sample of 60mm wide is used for the experiments, then by rotating the lead screws by a full turn results in a strain value of 1.67%. By using this model, the amount of strain can be altered to the required extent.

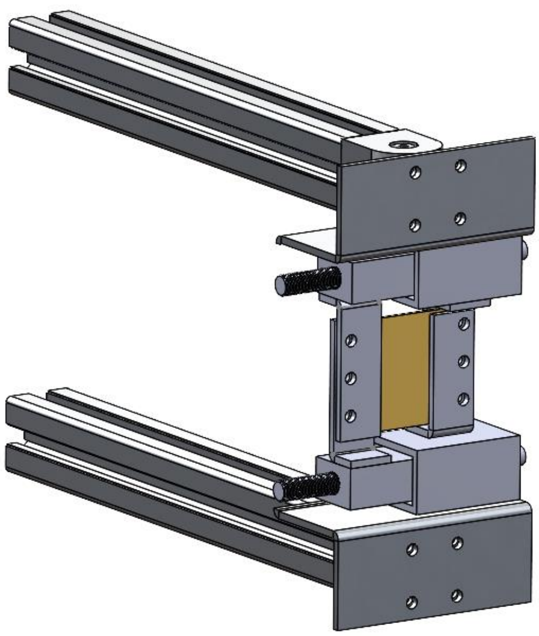

Figure 52 Model of the tensile clamp

Due to the COVID-19 regulations, the proposed model in Figure 52 could not be designed at the mechanical lab of the University of Twente, but a temporary clamp shown in Figure 53 was modelled to study the effect of strain on the ABS material. The maximum strain on the leading edge and allowable strain on the ABS material is 0.353% and 6% respectively. Table 7 shows the list of experiments proposed to study the effect of the strain on the rain erosion performance.

Table 7 Proposed experiments to study effect of strain

Material	Nozzle Diameter (mm)	Impact Velocity (m/s)	Impact Frequency (Hz)	Angle of Impact (w.r.t vertical)	Strain induced	Number of Impacts
Acrylonitrile Butadiene Styrene (ABS)	1.0	175	200	90^0	≈ 0%	200.000
					≈ 3%	200.000

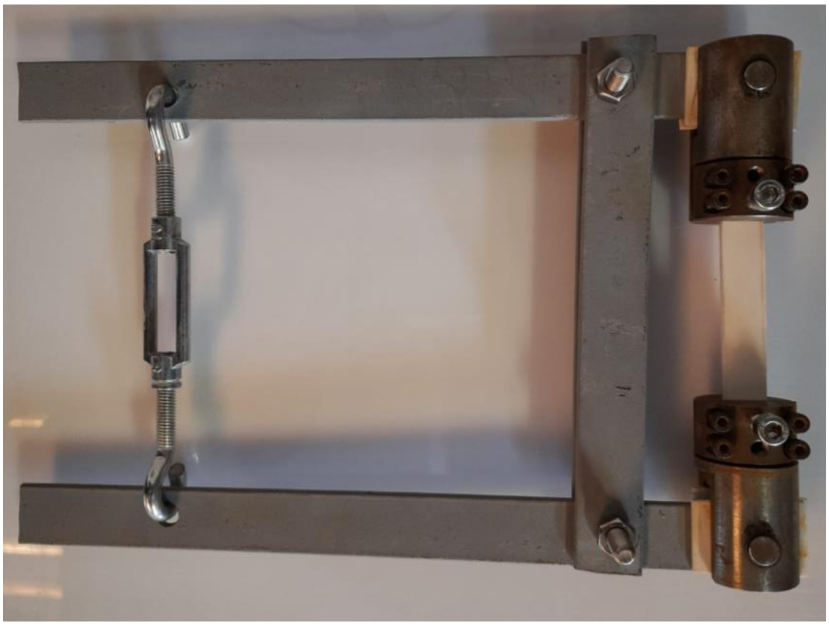

Figure 53 Temporary tensile clamp used for strain experiments

7.1 Discussion

The proposed tests were tried to perform using the temporary tensile clamp. Unfortunately, the tests could not be completed as the ABS sample used for the tests broke into half while conducting the experiments. This was because the sample was cut very narrow to fit it in the temporary clamp and the length of the sample was very long which probably induced heavy vibrations and oscillations in the sample as there was no support on the back side of the sample to withstand the heavy vibrations. Figure 54 shows the broken piece of sample lying in the water collector of the setup.

Figure 54 Broken Sample during the strain experiments

The number of impacts conducted during ≈0% and ≈3% strain was estimated to be 150.000 and 170.000 impacts respectively. The sample used for ≈3% strain lasted long because of the extra stiffness provided to the sample by the tensile pull, which was absent in the sample used for the ≈0% experiment. The laser intensity images obtained from the laser scanning confocal microscope can be seen in Figure 55.

From the Figure 55 it can be identified that the intensity of pitting is higher at ≈3% strain than that of ≈0% strain, which suggests that the material is prone to more damage when there is additional strain acting on it. Although there is a difference in the number of impacts in the test cases, the pitting intensity is comparably higher in the case of ≈3% strain. To understand the level of erosion, these test results can be compared to that of the results obtained from the experiments conducted with and without air blower.

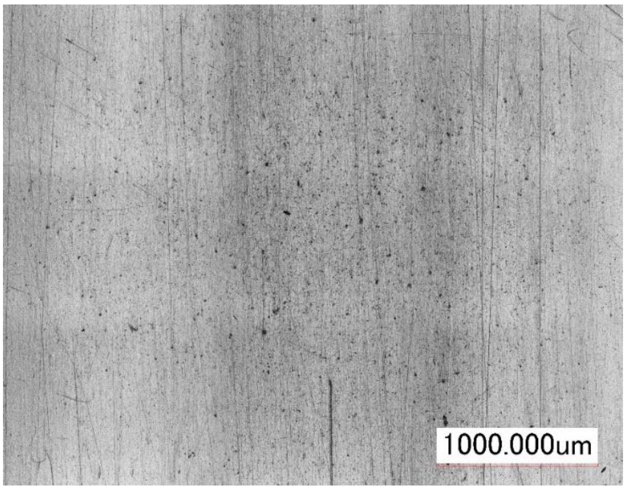

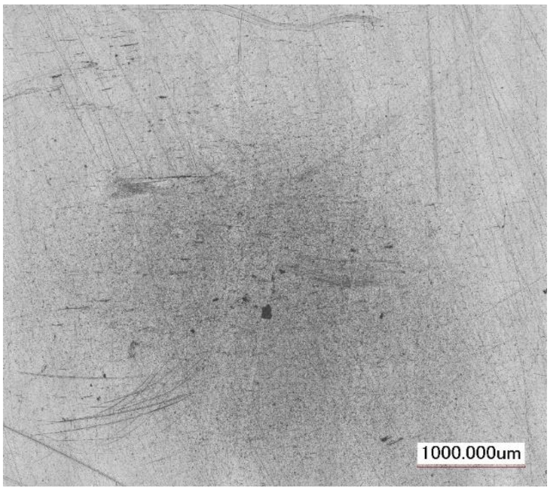

≈ 150.000 impacts, ≈0% strain

≈ 170.000 impacts, ≈3% strain

Figure 55 Laser intensity images of ABS samples

From Table 8 it can be identified that the volume loss of the sample with 170.000 impacts and a strain of ≈3% is higher than that of the volume loss of the sample with ≈0% strain. It can also be seen that the sample with 200.000 impacts without any strain has less volume loss than that of the sample with 170.000 impacts and ≈3% strain.Whereas, the volume loss at 200.000 impacts when an air blower is used is higher than that of the volume loss at ≈3% strain. The volume loss values show that the additional strain acting on the material makes a difference in the erosion behaviour when impacted with water droplets. The volume loss at ≈ 150.000 impacts with ≈0% strain is very close to that of the volume loss at 200.000 impacts in the case of without air blower. This proves that the rough estimation of number of impacts made in the case of ≈0% and ≈3% are reliable.

As already observed in Figure 50, the stress on the leading edge decreases gradually decreases from rotor to tip of the blade, whereas in Figure 51 the stresses decreased from a blade fraction of 25% from the root to the tip of the blade. These additional stresses in the material of the leading edge could be the reason for the rain erosion of the leading edge close to the root where the rotational speed is very low compared to that of the tip of the wind turbine blade.

Table 8 Volume loss of ABS samples at various impacts and strains

Material	Number of Impacts	Pressure of Compressed Air (bar)	Induced Strain	Volume loss (mm^3)
Acrylonitrile Butadiene Styrene (ABS)	≈ 150.000	N.A.	≈ 0%	0.00218
	≈ 170.000	N.A.	≈ 3%	0.00386
	200.000	N.A.	N.A.	0.00264
	200.000	2	N.A.	0.00457

More number of experiments with higher amount of impacts at different strain rates are needed to be conducted to validate the effect. The clamping system needs to be improved to prevent the specimen from breaking during the test.

During this research a tensile stress in in-plane direction was applied, which results in compaction in thickness direction. The water droplet impacts create compressive shock waves along the thickness of the material. Therefore, the additional stress in the material could have caused the observed early erosion in Figure 55. If the initial stress in the thickness direction is of tensile in nature, the maximum stress would have been lower, decreasing the extent of erosion due to the water droplet impacts. This technique can be tried by inducing a compressive strain in in-plane direction of the leading edge protection material which may decrease the extent of erosion on the surface of the material.

8 Conclusion

The objectives of this research were:

1. To identify the occurrence and development of the erosion due to the rain droplet impacts in the materials used for the leading-edge protection of the wind turbine blades.
2. To analyse the effect of the water layer present on the sample on the rain erosion.
3. To study the influence of additional strains on the rain erosion performance of the material used for the leading-edge protection of the wind turbine blades.

A literature study was conducted to understand the different stages of rain erosion on a material including the physics behind the droplet impact. A brief study on the existing RET methods and rain erosion parameters was conducted to identify the important rain erosion parameters.

Impact velocity, angle of impact, impact frequency and size of the rain droplet were identified to be the most important rain erosion parameters. To find out the damage initiation and its propagation, a pulsating jet erosion test setup which is available at University of Twente was used to conduct preliminary experiments on Acrylonitrile Butadiene Styrene (ABS) material, keeping the above-mentioned parameters constant. A Keyence VK9710 laser scanning confocal microscope was used to obtained the height maps of the surface of the tested samples. Various surface roughness parameters were studied and a methodology was created to analyse the results of the microscope using the skewness (Ssk) surface roughness parameter and material volume loss algorithm.

To understand the effect of water layer present on the surface of specimen, a water layer removal system using compressed air was designed and installed to the setup which blows away the layer of water stagnating on the sample. To achieve repeatability of the test results a second set of experiments was conducted which was not fruitful due to the broken setup. To reduce the total elapsed time of a single set of experiments new approaches based on “silicone imprints” and “clamping of the specimen” were proposed, out of which the new approach based on clamping of the specimen was more successful.

A final set of experiments to answer the first two questions of research were conducted. A qualitative and quantitative analysis were performed on the results of these tests. It was identified that the ABS material was under the stage of incubation until 600.000 impacts with intensified pitting on the surface of the material. The acceleration phase of the material was very short as a big crater was seen at 800.000 impacts. Later on, the ABS material is in the maximum state of erosion until 1.200.000 impacts with a volume loss of 0.078 mm^3. As the research is focussed to prevent the material from erosion damage, tests were not continued to identify the deceleration phase of the material.

While using a water layer removal system during the experiments, it was found that at 400.000 impacts the surface of the material consists of intensified pits and two very small craters which suggests that the material already passed its incubation phase. At 600.000 impacts a large crater was found which reveals that the acceleration phase of the material was ended. Later on, the material is in the maximum state of erosion until 1.200.000 impacts with a volume loss of 0.365 mm^3. The comparison of the test results of with and without water layer removal system revealed that the effect of water layer on the rain erosion of ABS material was evident.

While observing the laser intensity 10x images, it was identified that the erosion easily develops around the scratches due to the manufacturing defects or other reasons. This can be identified in Figure 56. The growth of craters tends along the scratches or defects in the sample.

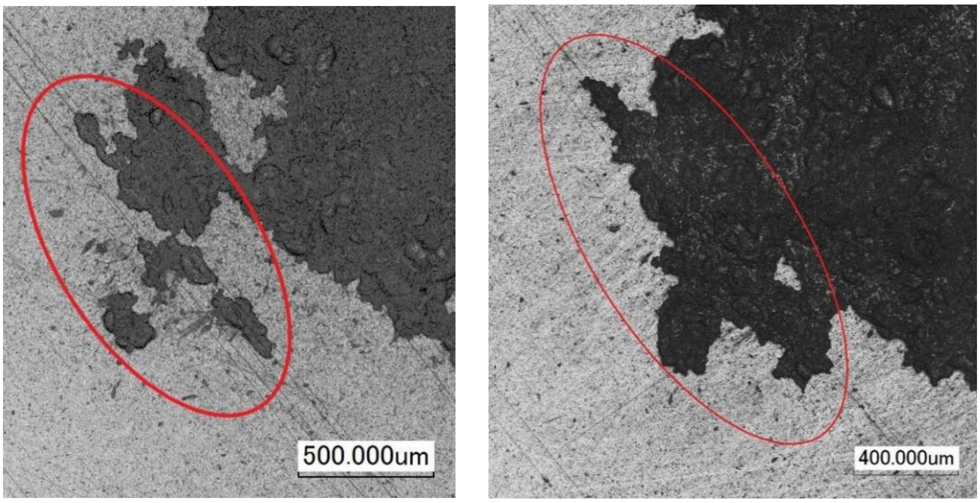

Figure 56 Erosion damage around the scratches

To evaluate the importance of additional strains in the material on the rain erosion performance, a temporary tensile clamp was designed to induce strain in the material during the rain erosion experiments. Tests were conducted using the tensile clamp at a strain rate of ≈0% and ≈3%. The qualitative analysis of these experiments showed that the intensity of pitting is high with a volume loss of 0.0039 mm^3 on the sample with a strain of ≈ 3% whereas the volume loss of the sample at ≈0% strain is 0.0022 mm^3. These results show that the additional strain acting on the material makes a difference in the material behaviour when impacted with water droplets.

The final conclusion of this research is that the incubation phase of the ABS material ends early when there are additional strains or there is no presence of water layer on the specimen, which results in severe damage in the material's life time. The experimental and analysis methodology used in this research can be applied on various materials to gain more insights of their erosion performance.

9 Recommendations

There is always scope for further development. Some of the noteworthy points for the future research are listed in this chapter.

- The tests during this research were conducted in an instalment of 200.000 impacts on different days to complete 1.200.000 impacts. This should be compared with the volume loss of the samples when all the 1.200.000 impacts were done at once, because the continuous water droplet impacts over a long period of time can induce additional strains in the material.
- The impact of the jet and lateral jetting after the impact while using the water removal system needs to be verified in order to check if there is any influence of the air flow on the water jet.
- The tensile clamp which was initially modelled needs to be prepared to perform full range of strain experiments.
- During the tests with water removal system, between 400.000 to 600.000 impacts a change in erosion behaviour was observed. Therefore, at 500.000 impacts a comparative study of (i) Without air blower, (ii) With air blower, (iii) With additional strain and (iv) With both additional strain and air blower can give in-depth knowledge regarding the incubation phase in various working conditions.
- In future research, tests in between 400.000 to 800.000 are to be prioritized to precisely identify the end of incubation and acceleration phase.
- During this research, it was found that the additional strain in the material has its effect on the rain erosion performance. Therefore, testing the thermoplastic material when bonded with the turbine blade backbone can give reliable results than that of testing one single layer of thermoplastic material.
- The results obtained from the tests conducted by using water layer removal system should be compared to the results of whirling arm setup to understand the significance of water layer in the practical application.
- The elapsed time of the experimental work can be considerably reduced if the PJET setup and the confocal microscope are located in a single facility, which allows to perform a greater number of tests.
- To perform iterations and testing at high number of impacts i.e., over 500.000 impacts in a short period of time a new test approach is required. In this approach the slow curing silicones and the new sample positioning approach mentioned in chapter 5.2 and 5.3 respectively of this report can be used together to achieve better results with reduced time spent on experiments. The flowchart in Figure 57 shows an example of succession of events during the

experimental flow while using the new test approach. E1 and E2 represent the number of the iteration during the test.

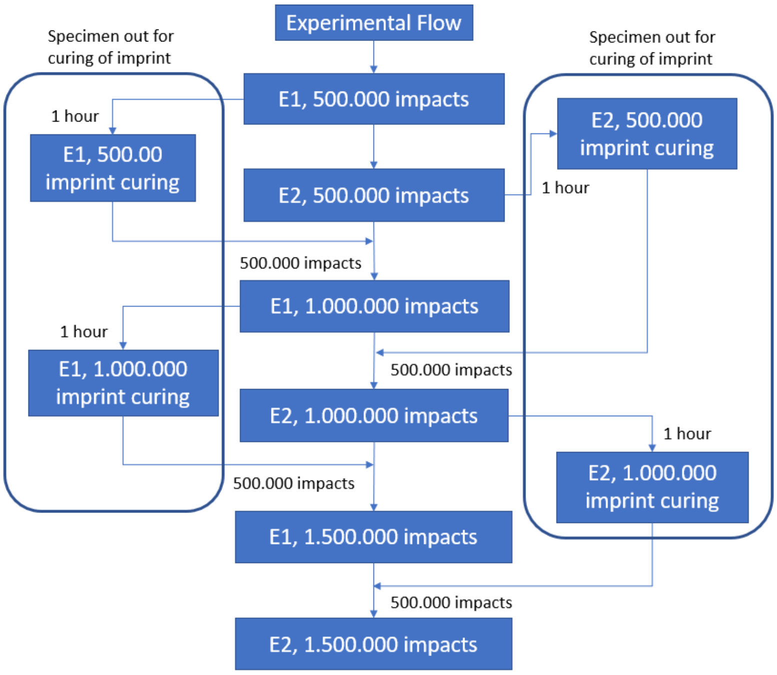

Figure 57 Example of experimental flow of the new test approach

Table 9 shows the comparison of various approaches discussed in this report. Based on the total time spent on the experiments, new sample positioning approach is the best approach when the PJET setup and the confocal microscope are in a single facility. Otherwise, the approach involving slow curing silicones and new sample positioning approach is the best approach to follow in order to reduce the amount of time spent on the experiments.

Table 9 Comparison of different approaches

Number of Impacts	Frequency (Hz)	Time spent on each test (sec)			
		Initial approach	Slow curing Silicones	New sample positioning approach	Slow curing silicones + New sample positioning approach
500.000	200	2500	6100	2500	3600
500.000		2500	6100	2500	3600
1.000.000		5000	6100	2500	3600
1.000.000		5000	6100	2500	3600
1.500.000		7500	2500	2500	2500
1.500.000		7500	2500	2500	2500
Total time (min)		500	490	250	324

10 References

1. Hannah Ritchie (2017). "Renewable Energy". Published online at OurWorldInData.org. Retrieved from https://ourworldindata.org/renewable-energy
2. EUROSTAT (online data codes: nrg_ind_peh, nrg_cb_e, nrg_105m) EU-28 electricity statistics. Retrieved from https://appsso.eurostat.ec.europa.eu/
3. Wind Europe. [2019]. Wind energy is the cheapest source of electricity generation. Retrieved from https://windeurope.org/policy/topics/economics/
4. The Angels of Science. [2017]. Ingenious techniques for increasing the power of wind energy technology. Retrieved from https://scientistmohamed.wordpress.com/category/renewable-energy/
5. Technology roadmap of wind energy 2013 edition, International Energy Agency (2013) 1-58, Paris, France.
6. S.A. Kalogirou, Chapter 13 - Wind Energy Systems, in: S.A. Kalogirou (Ed.), Solar Energy Engineering (Second Edition), Academic Press, Boston, 2014, 735-762.
7. GE Renewable Energy. [n.d.] Haliade-X offshore wind turbine. Retrieved from https://www.ge.com/renewableenergy/wind-energy/offshore-wind/haliade-x-offshore-turbine
8. L. Rampel, Rotor blade leading edge erosion – real life experiences, Wind Systems Magazine (Issue date 24.10.2012) 22-24.
9. Sareen A, Sapre CA, Selig MS (2014) Effects of leading-edge erosion on wind turbine blade performance. Wind Energy 17:1531–1542
10. Wind power engineering & development. [2016]. Easily applied covering could be the fix for leading edge erosion. Retrieved from https://www.windpowerengineering.com/easily-applied-covering-fix-leading-edge-erosion/
11. E. Tobin, T. Young, D. Raps and O. Rohr, "Comparison of liquid impingement results from whirling arm and water-jet rain erosion test facilities," Wear, vol. 271, no. 9-10, pp. 2625-2631, 2011
12. D.J. Pel, (2019). Designing and building an instrumented Rain Erosion Test set-up for wind turbine blades. University of Twente, Enschede, The Netherlands.
13. Elhadi Ibrahim M, Medraj M. Water Droplet Erosion of Wind Turbine Blades: Mechanics, Testing, Modeling and Future Perspectives. *Materials*. 2020; 13(1):157. https://doi.org/10.3390/ma13010157

14. R. Herring, K. Dyer, F. Martin, and C. Ward, “The increasing importance of leading-edge erosion and a review of existing protection solutions,” *Renewable and Sustainable Energy Reviews*, vol. 115, no. February, 2019, doi: 10.1016/j.rser.2019.109382.
15. Zhag,S. (2014). Accelerated rain erosion of wind turbine blade coatings. Kgs. Lyngby: Danmarks Tekniske Universitet (DTU).
16. DNV-GL. [2018] Testing of rotor blade erosion protection systems. Retrieved from https://www.dnvgl.com/rules-standards/
17. Tobin, E. F., Young, T. M., Raps, D., and Rohr, O. (2011). Comparison of liquid impingement results from whirling arm and water-jet rain erosion test facilities. Wear.
18. Bartolomé, L., & Teuwen, J. (2018). Prospective challenges in the experimentation of the rain erosion on the leading edge of wind turbine blades. Wind Energy. https://doi.org/10.1002/we.2272
19. Gunn, R.; Kinzer, G.D. The terminal velocity of fall for water droplets in stagnant air. J. Meteorol. 1949, 6, 243–248.
20. M H Keegan et al 2013 J. Phys. D: Appl. Phys. 46 383001
21. S. Hattori and M. Kakuichi, “Effect of impact angle on liquid droplet impingement erosion,” *Wear*, vol. 298–299, no. 1, pp. 1–7, 2013, doi: 10.1016/j.wear.2012.12.025.
22. K. Pugh, G. Rasool, and M. M. Stack, “Raindrop Erosion of Composite Materials: Some Views on the Effect of Bending Stress on Erosion Mechanisms,” *Journal of Bio- and Tribo-Corrosion*, vol. 5, no. 2, pp. 1–12, 2019, doi: 10.1007/s40735-019-0234-8.
23. O. Gohardani, “Impact of erosion testing aspects on current and future flight conditions,” *Progress in Aerospace Sciences*, vol. 47, no. 4, pp. 280–303, 2011, doi: 10.1016/j.paerosci.2011.04.001.
24. J. Zahavi, S. Nadiv, and F. Schmitt, “Indirect-damage-in-composite-materials-due-to-raindrop-impact_1981_Wear.pdf,” vol. 72, pp. 305–313, 1981.
25. J.F. Manwell, J.G. McGowan, A.L. Rogers. (2009). Wind Energy Explained: Theory, Design and Application, Second Edition. Wiley.
26. Surface Roughness Parameters – Tautology. (n.d.) Retrieved from https://www.keyence.eu/ss/products/microscope/roughness/surface/tab01_b.jsp
27. Surface Roughness Measurement – Parameters. Tautology. (n.d.) Retrieved from https://www.olympus-ims.com/en/metrology/surface-roughness-measurement-portal/parameters/#!cms[focus]=cmsContent14709&cms[tab]=undefined
28. Bharat Bhushan, Surface roughness analysis and measurement techniques (2001), Modern Tribology Handbook Volume 2, CRC Press, 2000, 6-7.

29. Tribology: Lubrication, friction and wear. [March 2017]. Typical surface roughness. Retrieved from https://tribos.wordpress.com/category/tribology/surface-roughness/
30. T.H. Hoksbergen et al 2020 IOP Conf. Ser.: Mater. Sci. Eng. 942 012023
31. D. Todd Griffith, Thomas D. Ashwill (2011). The Sandia 100-meter All-glass Baseline Wind Turbine Blade: SNL 100-00 (Report No. SAND2011-3779).